

See discussions, stats, and author profiles for this publication at: <https://www.researchgate.net/publication/348607458>

# Topical Review MicroLED technologies and applications: characteristics, fabrication, progress, and challenges

Article in *Journal of Physics D Applied Physics* · January 2021

CITATIONS

0

READS

7,729

3 authors, including:



Shuke Yan

Nanosys

6 PUBLICATIONS 114 CITATIONS

[SEE PROFILE](#)



Cameron Danesh

University of California, Los Angeles

14 PUBLICATIONS 107 CITATIONS

[SEE PROFILE](#)

Some of the authors of this publication are also working on these related projects:



III-V optoelectronic device design and fabrication [View project](#)



Design and fabrication of semiconductor electronics for neuromorphic circuits [View project](#)

## Topical Review

# MicroLED technologies and applications: characteristics, fabrication, progress, and challenges

Zhen Chen , Shuke Yan  and Cameron Danesh 

Glō-USA, Inc., 1225 Bordeaux Drive, Sunnyvale, CA 94089, United States of America

E-mail: [zchen99@gmail.com](mailto:zchen99@gmail.com) and [zhen.chen@glo-usa.com](mailto:zhen.chen@glo-usa.com)

Received 4 August 2020, revised 14 October 2020

Accepted for publication 2 December 2020

Published 14 January 2021



### Abstract

Micro light-emitting diode (microLED) technology is expected to be used in next-generation displays and other applications due to its many advantages. This paper categorizes, reviews, and analyzes the main challenges and technical solutions in the microLED displays manufacturing process, covering epitaxial growth, wafer fabrication, mass transfer, control circuit, and panel. In the overview section, the comparison between microLED, liquid crystal display, and organic light-emitting diode displays, as well as the various applications of microLEDs, are reviewed. In the same part, the specific challenges of microLED manufacturing are also discussed, including full-color operation, reduced external quantum efficiency (EQE), low-efficiency and low-yield mass transfer, and structure and process design from a system perspective. In the epitaxial growth section, the requirements, problems, and technical developments of epitaxial growth, especially the growth of AlInGaN red LED, have been reviewed. The microLED chip characterization and fabrication section present the reasons for the low EQE of microLEDs and the methods to overcome this problem. This section also includes the unique characteristics and theories of microLEDs, compared with those of traditional broad-area LEDs. Various mass transfer technologies are summarized in the mass transfer section. The design and operation mechanism of the microLED control circuit is discussed in the control circuit and panel section. This section also introduces the manufacturing and performance improvement of the backplane and the panel. The best way to use this review is to read the overview section first, get a big picture of microLEDs, read the chip section to learn about their special features and reasons behind them, and then go to the parts you are interested in.

Keywords: microLED, display, InGaN, AlInGaP, epitaxy, wafer fabrication, mass transfer

(Some figures may appear in colour only in the online journal)

## 1. Overview

### 1.1. Background

In terms of chip sizes, light-emitting diode (LED) can be divided into three categories: traditional broad-area LEDs larger than 200  $\mu\text{m}$ , mini-LEDs between 100 and 200  $\mu\text{m}$ , and microLEDs smaller than 50  $\mu\text{m}$ . Broad-area AlInGaN

ultraviolet, blue, green, white LEDs, and AlInGaP red LEDs have achieved huge success in general lighting, display backlighting, signaling, outdoor displaying, curing, and other applications. Mini-LEDs are used for backlighting applications such as high-end displays, high-dynamic-range (HDR) displays, and flexible displays [1]. In theory, microLED is suitable for all kinds of displays, including virtual reality (VR), augmented reality (AR), wearables devices, smartphones,

high-definition television (HDTV), etc. MicroLED is used as self-emissive pixels in a display, competing with organic LED (OLED) to liquid crystal display (LCD), where broad-area LEDs and mini-LEDs are used as backlighting. Therefore, microLED manufacturing and operation are different from the broad-area LED and mini-LED in many ways. Jiang's group proposed using InGaN microLED as display pixels and demonstrated a display with  $12 \mu\text{m}$  microLEDs in 2000 [2]. Many teams from universities and research institutes have been working in this field for a long time, including Dawson's group at the University of Strathclyde [3], Lau's group at the Hong Kong University of Science and Technology [4], and so on.

Since Apple acquired LuxVue to produce microLED displays in 2014, interest in microLED has grown dramatically because it is believed that Apple will use this novel display technology in its future versions of products, including iWatch, iPhone, and iMac. MicroLED may become the next generation of display technology because of its excellent optical and electrical characteristics, which have been proven in broad-area LED. If microLED succeeds in replacing LCD and OLED, it will be a new trillion-dollar market. Facebook-owned VR company Oculus acquired InfiniLED in 2016 and reached an exclusive agreement with Plessey to develop a microLED AR display in 2020. Sharp and Foxconn invested in eLux, a company assembling microLED display by self-assembly transfer technology, in 2017. Google invested in microLED company Glō AB (winner of an I-Zone honoree award at Display Week 2017, with Jasper display company), and Intel invested in glō's competitor Aledia [5]. Samsung partnered with Epistar and PlayNitride to produce microLED TVs. Today, most of the display and LED companies have announced that they are developing microLEDs technology.

Despite the many challenges in microLED displays manufacturing, Samsung has demonstrated a 146 inch microLED TV called The Wall in 2018. Because it used traditional SMD-packaged LEDs with chip sizes larger than  $0.1 \text{ mm}$ , it was not strictly qualified for microLED [5]. Sony demonstrated a flat panel display up to  $21 \text{ m} \times 5.5 \text{ m}$ , in which  $30 \mu\text{m}$  microLEDs were used in 2019. It shows superior performance than LCD, with 3.5 times higher contrast, 1.4 times better color range, ten times faster response time, and a wider viewing angle of 180°. Furthermore, there is no size limit for microLED flat panel displays because they are constructed seamlessly from many smaller modules. These demonstrations show that microLED is a promising candidate for next-generation display technology. Theoretically, microLED has better performance than LCD and OLED. Its advantages and disadvantages are discussed in section 1.2.

## 1.2. Advantages and disadvantages of microLED

As the mainstream display technology, LCD's main disadvantages are slow response, poor efficiency, low color saturation, etc. OLED displays have the advantages of self-emission: wide-angle, high-contrast, high-efficiency, fast response, and so on. As a result, OLED is being used in the latest smartphones and TV monitors. Thanks to the same self-emissive

technology, microLED has all the advantages of OLED over LCD. Besides, based on the characteristics and performance of broad-area LEDs, microLED can theoretically provide higher brightness, higher contrast ratio, better resolution, faster response, longer lifetime (LT), better environment stability, and wider viewing angles than LCD and OLED. Table 1 lists the comparison of LCD, OLED, and microLED, which will be discussed one by one.

As for brightness, microLED is two orders of magnitude brighter than LCD and OLED. LCD loses brightness due to the required optical system, including polarizers, color filters, etc. The presentation of glō's smartwatch-size display shines with 10 000 nits, while the equivalent OLED would burn out in a few seconds [6]. Low luminance is also a major obstacle to using OLED in outdoor applications such as AR, VR, smartwatches, and mobile phones.

Ambient contrast ratio (ACR) is an essential specification for outdoor applications. For example, it is sometimes difficult for customers to read the screen of a smartphone or tablet with an OLED display panel under high ambient light. In theory, both microLED and OLED can achieve an infinite or very high contrast ratio because the black pixels are turned off, as shown in table 2. However, the ACR of microLED is much higher than that of OLED because the microLEDs brightness is much higher.

Regarding pixel per inch (PPI) and pixel size, Mojo display demonstrated a 14 000 PPI monochrome microLED display, ten times higher than OLED and LCD, which means that microLED chips can be as small as one micron. The PPI of LCD is low due to its mechanism. The nature of OLED materials makes it incompatible with conventional microfabrication processes [7]. Therefore, reducing the OLED pixel size to increase the PPI is challenging. In large screen displays with low PPI, small subpixels mean that the space between the chips is large. Therefore, the microLED array can integrate sensors and divers to achieve multi-functions such as finger-print identification, touch screen, and gesture control. In such large displays, the cost of the LED semiconductors is a significant portion of the Bill of Material. Therefore, the smaller subpixel is key to the commercialization of such displays.

Concerning reliability and environmental stability, AlInGaN and AlInGaP are grown at high temperatures. As a result, they are very stable at room temperature and can operate in a broader temperature range of  $-100^\circ\text{C}$ – $120^\circ\text{C}$ . The LT of the broad-area III-V LED exceeds 100 000 h. The LT of the microLED is even longer than the broad-area LED due to better heat dissipation. OLED can only operate in a narrow temperature range because of the temperature limitation of organic materials. Besides, OLED has a significantly shorter LT due to unstable materials and degradation during operation [8]. Due to OLED's poor thermal stability, the necessary encapsulation process increases the cost and complexity of OLED manufacturing [9]. Since the blue OLED material deteriorates very rapidly, in some OLED displays, compensation circuitry is necessary to maintain an acceptable performance level over the life of the product. In particular, while typical OLEDs can hardly survive at a current density of  $80 \text{ mA cm}^{-2}$  for over 100 h, microLEDs have been shown

**Table 1.** Comparison between microLED, OLED, and LCD.

Item	MicroLED	OLED	LCD
Mechanism	Self-emissive	Self-emissive	Backlighting and color filter
Luminance	Max. $>10^5$ nits (full color)	Max. $<5 \times 10^3$ nits (full color)	Max. $7 \times 10^3$ nits (full color)
Contrast ratio	$>1000\,000:1$	$>10\,000:1$	5000:1
PPI	Max. 30 000 PPI	Max. 1433 PPI	Max. 806 PPI
Pixel size	Min. submicron	Min. 18 $\mu\text{m}$	Min. 32 $\mu\text{m}$
Compactness	High	Medium	Low
Lifetime (LT 90%)	$>100\,000$	10 000	30 000–60 000
Operation temperature	$-100^\circ\text{C}$ – $120^\circ\text{C}$	$-50^\circ\text{C}$ – $70^\circ\text{C}$	$-20^\circ\text{C}$ – $80^\circ\text{C}$
View angle	Max. 180°	Max. 89°	Max. 89°
Environmental stability	High	Low	Medium
Response time	Ns	$\mu\text{s}$	Ms
Enhanced function	High	Medium	Medium
Power consumption	Low (in theory)	Medium	Medium
EQE	10%–30% ( $\sim 80\%$ in theory)	10%–40%	5%–12%
Cost	High	Low	Low

**Table 2.** Comparison of microLED application requirements.

Application	High PPI		Low PPI		
	AR/MR/VR/Projector	Vehicles	Wearables/Smartphones	Laptop	TV
PPI	>2000	>150	>350	>250	>100
Chip size (um)	<5	<100	<30	<30	20–80
Brightness (nits)	>5000	>5000	>1000	>500	>500
Contrast Ratio	>100 000:1	>100 000:1	>100 000:1	>100 000:1	>10 000:1

to survive at  $3.5\text{ kA cm}^{-2}$  for over 300 h due to their stability under high power densities [10, 11].

As for the response time, due to the high electron mobility, the switching speed of microLED is in the order of nanoseconds, while OLED and LCD are in the order of microseconds and milliseconds, respectively. This feature is significant for visible light communication (VLC) application. Some proprietary designs and processes are utilized in EPI structures, wafer fabrication, and driver circuits further to improve the response speed of microLED in VLC. HDR display, such as AR, MR displays, also prefer fast response because these devices need more pixel per inch and more frames per second for convenience and safety [12].

For compactness, self-emission and small pixels size are essential. The LCD requires a separate light source and complex optics, resulting in poor compactness. Both microLED and OLED are self-emissive, but the pixels of microLED are smaller than those of OLED.

MicroLEDs have the advantage of a wider viewing angle than LCD and OLED. Sony showed a wide-view angle TV, whose images look the same from different angles. Depending on display design and application, the light emission angle of microLED can also be adjusted by integrating optical components to match the requirement in narrow view angle applications.

Interestingly, the initial and primary driving force behind microLED displays is higher theoretical efficiency than LCD and OLED technology, reducing power consumption, and providing smaller batteries for wearable displays [13].

However, today's microLED has lower efficiency and higher power consumption compared to OLED and LCD due to the sidewall defects effect. Higher efficiency and lower power consumption have been claimed and expected based on the performance of broad-area LEDs. Therefore, high external quantum efficiency (EQE) and low power consumption of microLED are marked as 'In Theory' in table 1. The reduced efficiency is a significant challenge for the development of microLED and will be discussed in detail in the following sections. We believe that this problem can be solved in the future and eventually become an advantage with technology development.

Today's cost of microLEDs is prohibitive to commercialization. As a developing technology, each process has problems that impact yields. Therefore, the cost of microLED display products will require significant development time before it meets the required commercialization targets. On the other hand, the economies of scale that are enjoyed by LCD and OLED will also reduce microLED costs once the technology is scaled into the market. Although Sony and Samsung have demonstrated giant displays based on microLED technology, the price of microLED TVs far exceeds that of LCD and OLED TVs on the market.

### 1.3. Applications of microLED

As a result of the above advantages, microLED has a tremendous opportunity to replace LCD and OLED, and occupy all display applications, including AR, VR, MR,

wearables, smartphones, automobiles, laptop screens, TVs, as well as other novel applications.

**1.3.1. Display applications.** The microLED display applications can be classified into high PPI and low PPI, as shown in table 2. Each application takes advantage of some characteristics of microLED.

The PPIs of the Apple iPhone 11 Pro and Samsung Galaxy S9 is 456 and 567, respectively, which are high enough. Although people with perfect eyesight of 20/20 vision can read 720 PPI at 1 ft viewing distance, humans can usually see up to 300 PPI at 2.5 ft. PPI is critical in AR, VR, and MR applications because the images are projected and seen through optical lenses. Increasing the PPI from 400 to 1000 may not be noticeable in low PPI display but makes high PPI applications such as head-mounted displays (HMD) and projector different. The advantages of microLED are well reflected in AR, VR MR, and projector applications. Therefore, we compare the application of LCD, OLED, and microLED in these areas in more detail.

Images of HMD, AR and VR often overlap with the environment. Hence, their general requirements are high contrast of 100 000:1, high brightness of  $>5000 \text{ cd m}^{-2}$ , high PPI of  $>2000$ , lightweight, compact size, long operating time, high power efficiency, and fast response [14]. Head-up displays (HUD) in automobiles have similar requirements, but the PPI requirement is lower. Although liquid crystal on silicon microdisplay does not meet most of the above requirements, they are widely used in HMD and HUD because there is no better alternative. More than 90% of the initial light projected into the system is lost due to the complex imaging optics in reflective-style LCD. Therefore, LCD is not suitable for HMD and HUD. OLEDs are increasingly used in wearable AR systems because of the low brightness loss and the opportunity to simplify the optical systems significantly. As a direct emission technology, microLED has the same advantages as OLED but with far higher brightness and ACR. MicroLED is superior to OLED in all characteristics and performances because the quality of III-V semiconductor crystals is much better than that of amorphous organic materials. Among them, high brightness is the main advantage of microLED. For example, high-end glass-based AR/MR and HUD devices require a transparent display and a high brightness of 100 000 nits to view in an outdoor environment. This brightness can only be provided by microLEDs.

Interestingly, the two most significant challenges in microLED application, namely EQE and mass transfer defects, can be far less difficult in HMD, HUD, and projector fabrications. Firstly, the monolithic integration, rather than the more difficult pick-and-place process, can be utilized because of the small panel size. Moreover, these panels operate at high current densities to get high brightness. Sidewall defects have a relatively small impact at high current density because the sidewall defects can be saturated at higher current. After the sidewall defects are saturated, the luminance of microLED could be higher than that of broad-area LED at the same high current density due to the lower efficiency droop

in microLED. Overall, microLEDs have higher brightness, higher ambient contrast, higher compactness, more robustness, better environmental stability, and a more comprehensive operating temperature range, vital for outdoor applications. For high-PPI applications, no technology is better than microLED technology.

Based on the above reasons, the product strategy of microLEDs in display applications is to develop high PPI applications, including AR, MR, VR, wearable devices, and projectors, as the first-generation products. Automotive HUDs with similar requirements but low PPI can become the next generation of products. Since many problems need to be resolved before mass production, it will take more time to develop other low-PPI consumer electronics products with huge markets, such as smartwatches, smartphones, and HDTVs.

Tiny microLEDs can be bonded to flexible or stretchable substrates to make special displays such as curved displays, foldable smartphones, and wearable electronics. Park demonstrated the flexible array of AlInGaP orange and red microLEDs for the first time [15]. A transparent flat panel display can be realized when such a small microLED array adheres to a transparent substrate at a low fill factor. PlayNitride displayed an impressive transparent and flexible display, a genuinely see-through installation, and won a small booth award at SID 2019. The combination of low PPI configuration and high brightness can make a transparent display for vehicle navigation and heads-up display applications.

**1.3.2. Other novel applications.** MicroLED has potential in biomedical and health applications due to its comparable size with neurons, high response frequency, flexible display, and array integration [16]. It can be used to aid people with visual or hearing impairments [17]. Such neural stimulation, interface, and optogenetics have been demonstrated by replacing the traditional electric stimulator with a light on sensitized living neuron cells as early as 2008 by Dawson's group [18]. A microLED array implanted into a rat for neuron stimulation with wireless control has been demonstrated recently [19].

MicroLED may even achieve a naked-eye three-dimensional display, which may be the third-generation display after the next-generation microLED displays we are discussing. El-Alpaslan *et al* demonstrated the light field display shown in figure 1 [20]. Full parallax displays were considered impractical because displays required a large amount of data bandwidth and the complicated hardware with the existing display technologies. MicroLED with features of small pixel pitch, self-emission, high brightness, and high efficiency makes a small and compact light field display system possible [21].

VLCs have been used in both free space and optical fibers. Optical fibers links can be used in home networks and automotive applications. The sub-nanosecond response time of microLED makes it the right source for VLC. Furthermore, microLEDs provide large bandwidth and the capability of readily being formed in large array configurations

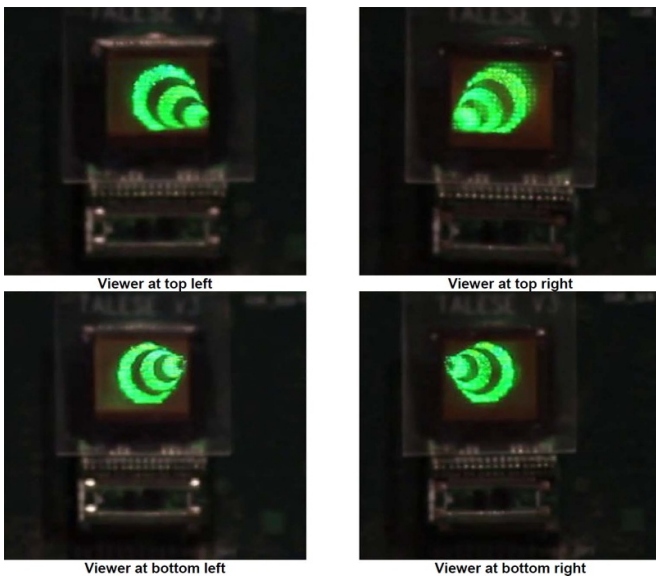


**Figure 1.** A parallax cone image is realized by microLEDs viewed from various angles. Reproduced with permission from [20]. © 2015 SPIE.

[22]. Parallel data transmission and equalization can allow data transmission rates higher than 1 Gbps [23]. Connecting with the advanced modulation, a violet microLED achieved a data transmission rate of up to  $11.95 \text{ Gb s}^{-1}$  [24]. Also, higher brightness than broad-area LED at high current density is a significant advantage of microLEDs in the application of VLC, as one of the disadvantages of VLC is the short communication distance.

#### 1.4. Challenges

Despite its many advantages and potential applications, it is unsure whether microLEDs will be the next generation of display technology due to many problems. Even if it can replace the current display technology, there is no agreement on the correct technical approach and the biggest challenge to realize a microLED display. For example, some argue that the challenges are mass transfer, the manufacture of thin-film transistor (TFT) substrates, and full-color implementation [25]. Others believe the main issues are efficiency due to poor p-type conductivity and the etched region to the active area ratio [26].

We think the top three challenges are three new problems in microLED application: mass transfer, low efficiency of a tiny chip, and systematic design of structures and processes for each component of the display system, to realize a well-optimized and high yielding component set and assembled display.

**1.4.1. Mass transfer.** 4K HDTV has approximately 25 million chips of  $3\text{--}10 \mu\text{m}$ , which must be assembled with a placement accuracy of  $1 \mu\text{m}$  at a throughput exceeding 100 million microLED chips per hour with yield  $>99.9999\%$ . For the 8K display, the chips number increase to 100 million. Transfer and assembly are generally regarded as the

most substantial technical challenges to overcome to enable microLED manufacturing. Many companies and research groups are working on it and making significant progress.

The methods used to assemble microLEDs on a panel are diverse, given the variety of innovations from companies working on the technology. However, it helps to divide the techniques into indirect pick-and-place vs. direct wafer-scale transfer, also called monolithic integration. Indirect transfer techniques typically include the assembly of microLEDs on a carrier substrate, print head, or a cartridge. The monolithic integration techniques utilize typical wafer-to-wafer or die-to-wafer type equipment and process with some customization to match the technique to the microLED wafer design and materials. The choice of each technique and its deployment are primarily driven and impacted by the target PPI and size of the display that the company intends to build. Consumer electronic displays of  $\sim 1''$  and above, with PPI in 100s vs. near-eye displays at sizes of  $<1''$  with  $\text{PPI} > 2000$ , introduce different demands and constraints on the transfer technique.

For consumer electronics applications such as smart-watches, smartphones, and larger displays, standard TFT backplanes similar to those used in OLED displays are necessary for cost reasons. The large surface of the display makes the use of CMOS as a backplane impossible from a cost point of view. Given the large area, the cost of the microLEDs in the Bill of Material is of key concern. Therefore, one must reduce the chip size to  $<10 \mu\text{m}$  to minimize the microLED costs. The chips must be fabricated densely packed on the wafer and then assembled on a much bigger display surface area sparsely distributed. For these larger displays, typically indirect transfer techniques. Examples of such techniques include MEMS-based carrier print heads used by LuxVue, polymer print heads used by X-celeprint, or cartridges used by Rohini and PlayNitride.

On the other hand, for near-eye displays such as AR and VR where the PPI requirement is  $>2000$ , CMOS backplanes are necessary due to high PPI, which cannot be achieved with TFT. The cost of CMOS backplanes is supportable in these applications since the display size is small. In this case, the density of the microLEDs on the wafer can be the same as that of the display. Hence, a high precision wafer-to-wafer or die-to-wafer assembly technique can be used. Plessey demonstrates an example of this. All these techniques to date have produced monochrome displays only. The expectation is that such monochrome displays can be assembled as RGB with the further integration of color converting quantum dots (QDs). Glō takes microLEDs and places them on both CMOS and LTPS backplanes to make displays of various resolutions and panel sizes [6]. The current transfer yields are high enough to make some parts; now, Glō focuses on making zero-defect panels [6].

Other examples include fluidic transfer used by e-Lux, or avoiding the need for transfer proposed by Lumiode, who aims to build the backplane stack directly on the microLED wafer. They deposited layers of silicon dioxide and amorphous silicon on the top of the premade microLED array and transferred them to polycrystalline Si TFT by laser [27].

**1.4.2. Reduced EQE with a shrunken chip size.** A problem caused by the small chip size is reduced EQE. MicroLED chips must be decreased to  $<5\text{--}10 \mu\text{m}$  to minimize costs, to compete with LCD and OLED TVs in terms of price. The EQE of a broad-area blue LED can reach 80%; however, the EQE of blue  $5\text{--}10 \mu\text{m}$  microLED is usually  $\leq 20\%$ . At such a level, microLED cannot achieve the critical promise of better efficiency than LCD and OLED. The problem of low EQE in microLED must be solved before entering the highly competitive consumer electronics market. Due to small chip dimensions and low applied current in large displays, microLED operation is impacted by severe sidewall effects related to defects such as dangling bonds, contaminations, or structural damages in which nonradiative carrier recombination dominates. These defects mainly come from the mesa etch. Glo has successfully designed and made microLEDs working at low current densities, two orders of magnitude smaller than that in solid-state lighting (SSL) [6]. Solutions include new LED structures, chip architecture designs, and process improvement to reduce the effect of sidewall defects. Dramatic progress has been made to improve EQE. The best reported blue microLED EQE is 33% for  $20 \mu\text{m}$  and 25% for  $5 \mu\text{m}$  [28]. Other methods include nanowire (NW) LED and LED grown on patterned templates, in which there are no sidewall damages [29]. Detailed theories and various technologies to improve microLED EQE will be reviewed later.

**1.4.3. Structure and process design from a system perspective.** Traditional LED manufacturers have little experience in display manufacturing and vice versa. MicroLED displays manufacturing requires expertise in several main areas: epitaxy, wafer fab, chip transfer, backplane, and display, which is a long chain. There is no universally accepted technology to manufacture microLED displays today. Different groups use various techniques in each process. For example, red emissions can be achieved by AlInGaP-based red LED, or blue/UV converted red via QD phosphor, or InGaN-based red LED on sapphire/Si substrates or nanostructures. Another good example is that different companies and universities have developed more than a dozen mass transfer technologies. The mainstream technologies in each process, from epitaxy to panel, are listed in table 3.

The structure and process design to produce microLED displays need to be considered an overall system because each step interacts with the other steps. How to transfer the microLED array will decide the epi structure and chip architecture. For example, laser liftoff associated transfer technology cannot use InGaN-on-Si or AlInGaP epitaxy technology. It is also true in circuit design. RGB's voltage difference must be considered if the RGB light emission is from AlInGaN and AlInGaP LEDs separately. If the RGB is realized from the color conversion of blue/UV microLEDs, all the color subpixels have the same voltage.

We believe that designing the structure and process of each step from a system perspective is one of the main challenges in microLED manufacturing. It is best to develop the structure and process of each step according to the final product with

**Table 3.** The existing technologies in each step of the microLED manufacturing chain.

Process	Mainstream technologies
Epitaxial growth	AlGaN red vs. AlInGaN red vs. converted red from UV or blue Sapphire substrates vs. Si substrates Planer LED vs. nanostructures vs. regrowth on patterned templates
Wafer fabrication	Flip-chip vs. vertical chip (More details like PECVD vs. ALD passivation, etc)
Mass transfer	Direct monolithic integration vs. Indirect pick-and-place Mass transfer technologies
Panel	High PPI vs. low PPI panel LTPS vs. CMOS Active Matrix vs. Passive Matrix PMOS vs. NMOS

the overall picture and actual situation in mind. For example, some may argue that if the final product is VR, in theory, the best combination of processes is InGaN RGB wafer on Si substrates, vertical thin film chip, direct wafer-to-wafer transfer onto a CMOS backplane. InGaN-on-Si RGB LEDs have a small mismatch with Si CMOS. A Vertical chip is necessary to make a small chip for high PPI and to remove the absorptive Si substrate. The direct wafer-to-wafer transfer is good enough to ensure the transfer speed, yield, uniformity, and low cost because of the small panel size. COMS guarantees fast response and compensation function. In practice, InGaN blue and green LEDs on sapphire are usually used because there are not many companies with GaN-on-Si technology. AlInGaP red LED typically replaces InGaN red LED because of low EQE and big blueshift at high current density in the InGaN red LED.

**1.4.4. Defects management.** The number of defects in current commercial flat panel displays is almost defect-free. Defects are inevitably introduced in each LED manufacturing process. A solution to minimize and control defects in microLED is critical. The yield of broad-area LED products can reach 100% because bad chips are filtered out in tests. Broad-area LEDs are tested in key steps, and only qualified wafers, chips, or modules can pass, and then proceed to the next process. Smaller microLEDs mean that thousands of times more testing than broad-area LEDs in one wafer. This problem can only be solved from a system perspective, covering various solutions from start to finish.

Firstly, the low-defect process needs to be elected in each step of the long manufacturing chain. For example, epitaxial growth should choose proper MOCVD equipment and processes that generate fewer defects, even at a price of lower efficiency. Secondly, new test methods need to be developed in each key process, especially in wafer manufacturing. MicroLED is too small to be tested by traditional probes. Conventional probes are too large to damage the chip and block light. High-speed contactless inspection and testing are necessary at four main steps during the entire manufacturing: epi wafer, chip-on-wafer, chip-after-transfer, and pixel-in-panel. However, there is no such commercial fast

and contactless characterization equipment available yet. The known-good-die (KGD) mapping must be obtained via these tests to handle the lousy chip in the subsequent process. Thirdly, technology to manage defects in the final product, a panel, needs to be developed, which is still a puzzle. One of the current solutions is to repair the dysfunctional pixel by repeat transfer. Another is redundancy by doubling the number of microLEDs in each subpixel. Systemic engineering that covers all microLED display manufacturing processes must be applied. Improving each process can simplify subsequent processes. For example, improved epitaxial growth uniformity can eliminate the need for wavelength and brightness sorting.

**1.4.5. How to realize red emission.** There are mainly three methods to realize red emissions from microLEDs. High-efficiency InGaN blue LED with an EQE of 84.3% [30] and AlInGaP red LED with EQE of 55% [31] have been demonstrated. Therefore, people intend to use the AlInGaP microLED as the direct red-light emission source. It is a correct choice for red microLED with a size  $>20\text{ }\mu\text{m}$ . However, AlInGaP red microLED has some problems compared to AlInGaN red microLED when the chip is  $<5\text{ }\mu\text{m}$ . The issue is that the efficiency of AlInGaP microLED drops very fast with pixel size shrink, resulting in a very low EQE for chip smaller than  $2\text{ }\mu\text{m}$ . Carrier diffusion length is smaller in III-nitride LED than those in phosphide due to the lower carrier diffusion coefficient in III-nitride [32]. The reported ambipolar diffusion coefficients of InGaN multiple quantum wells (MQWs) and AlInGaP MQWs are  $0.1\text{--}1\text{ cm}^2\text{ s}^{-1}$  [33, 34] and  $\sim 3\text{ cm}^2\text{ s}^{-1}$  [35, 36], respectively. Moreover, InGaN LED has a much smaller surface recombination rate of  $\sim 3 \times 10^2$  to  $\sim 10^4\text{ cm s}^{-1}$  than that of AlGaInP red LEDs ( $\sim 10^6\text{ cm s}^{-1}$ ) [32, 37, 38], which makes the sidewall effect in AlGaInP red microLED much severer than that in InGaN one. These behaviors make it possible for InGaN red microLED to have a higher EQE than AlInGaP red microLED. UCSB reported that green microLEDs are less sensitive to efficiency reduction with the shrinking size, thus attaining higher EQEs than blue microLEDs smaller than  $10\text{ }\mu\text{m}$  despite lower green efficiencies in the broad-area LEDs [39]. This is explained by smaller surface recombination resulting from the enhanced localization in the higher indium composition MQWs. That means the red InGaN microLED below  $10\text{ }\mu\text{m}$  may have higher EQE than InGaN green/blue and red AlInGaP red. The tendency of the EL peak wavelength shift with temperature ( $0.085\text{ nm K}^{-1}$ ) of  $630\text{ nm}$  InGaN red LED is smaller than that ( $0.137\text{ nm K}^{-1}$ ) of the  $630\text{ nm}$  AlInGaP red LEDs because the carrier overflow is induced by the smaller band offset between the active and barrier layers in AlInGaP material [40]. Therefore, InGaN-based LEDs are better candidates for temperature stability applications. In addition, using the InGaN red LED has other advantages since all the RGB microLED devices are from the III-nitride with the same characteristics and driving configurations in the system. It simplifies microLED fabrication, transfer, and backplane technologies. Therefore, some groups are developing an InGaN RGB microLED display.

The direct RGB emission microLEDs' manufacturing process is very complicated, no matter from AlInGaN or

AlInGaP. There are difficulties from epitaxy, wafer fabrication, through mass transfer and control of each subpixel. To avoid these problems, a color conversion method has been proposed by converting  $450\text{ nm}$  blue or  $410\text{ nm}$  UV microLED into RGB in displays [41]. Conventional phosphors cannot be used as color conversion materials due to their large size. QDs are only several nanometers in size and can emit light with characteristic frequency by precisely adjusting their size, shape, and composition. Compared with LCD, mini-LED LCD, and OLED displays, QD color conversion (QDCC) microLED displays have the advantages of narrow emission linewidth, large-area color gamut, low cost, and simple process. QDTV adopts QDCC technology and is one of the mainstream TVs in the market. This means that QDCC microLED display technology is feasible to make HDTV. Simultaneously, the color conversion method has low conversion efficiency, uneven emission pixels, color/light crosstalk, and a low LT.

**1.4.6. Other challenges.** Many other small challenges in each process also need to be addressed. In epitaxial growth, the wavelength uniformity and defects density must be improved to an order of magnitude lower than current specs used in broad-area LED. The epitaxial structure needs to be designed so that the peak EQE is positioned at the desired operating current density, which can be two orders of magnitude lower in TV or two orders of magnitude higher in VLC than the broad-area LEDs used in general lighting. The reduction of the wavelength drift with current density and the reduction of the full-width half maximum (FWHM) are also challenges in the LED structure design. In circuit design, it is necessary to have a compensation circuit to improve the wavelength and luminance uniformity of the microLED display. Likely, the microLED uniformity is not far worse than OLED fabricated by large-area deposition, but further data is needed for optimized circuit designs. As a result, amorphous silicon or low-temperature polycrystalline silicon (LTPS) TFT driver for OLED may not be sufficient for microLED control.

## 2. Epitaxial growth for microLED

InGaN MQWs are usually grown on sapphire substrates for blue and green microLEDs, and AlGaInP MQWs are grown on GaAs substrates for red microLEDs by MOCVD. These growths have been well developed. Therefore, we do not discuss growth details but focus on the new growth challenges and technologies related to microLEDs. The epitaxial growth of RGB wafers remains a crucial technology in microLEDs fabrication because of new requirements in microLEDs, novel technologies to realize RGB colors, and the need to improve EQE at small chip size.

### 2.1. Requirements and challenges in epitaxial growth

The specifications of epitaxial wafers for microLED applications can be divided into three categories. The first

category is the optoelectronic characteristics, including efficiency, forward voltage, leakage current, electrostatic discharge, etc, which are the same as the broad-area LED in SSL application.

The second category is more tight specifications than broad-area LED, but there are opportunities to achieve through equipment and process improvements. These specs include bow, thickness uniformity, wavelength uniformity, and defect density. Bow control is essential to maintain the back-end process. Conventional 6 inch LEDs have a typical bow of  $<150 \mu\text{m}$ , but the wafer bow needs to be reduced to  $<50 \mu\text{m}$  in microLEDs fabrication because of the requirement of the stepper lithograph process. The wafer thickness uniformity criteria need to be tightened to facilitate etching, multiple color transfer, and bonding. The thickness standard deviation spec of a 6 inch wafer for broad-area LED in SSL application is usually  $<0.5 \mu\text{m}$ , but for microLEDs, it generally decreases to  $<0.1 \mu\text{m}$ .

For microLED, there are no sorting and binning steps before the mass transfer, no matter pick-and-place or monolithic transfer. Therefore, high wavelength uniformity and low defect density are two critical criteria for the subsequent production processes and final products. It is not easy to improve these two features. The demand for the color uniformity in a stamp usually originates from the CIE 1976 (uniform chromaticity scale) UCS. The stamp is typically  $10 \text{ mm} \times 10 \text{ mm}$ . The color area should be within a white point tolerance of  $\pm 0.003$ , corresponding to around  $\pm 2 \text{ nm}$  for RGB [42]. Aixtron planetary reactor demonstrates excellent in-wafer, wafer-to-wafer, and run-to-run wavelength standard deviations with values of  $\sigma_{\text{in wafer}} \sim 0.3 \text{ nm}$ ,  $\sigma_{w/w} \sim 0.3 \text{ nm}$ , and  $\sigma_{R/R} \sim 0.2 \text{ nm}$  for  $8 \times 6''$  configuration [43].

The defect requirement in a stamp is  $\leq 20 \text{ ppm}$  based on ISO 9241. Thus, EPI wafers' criteria are using stamp-free of defects with size  $\geq 1 \mu\text{m}$  [42]. If the yield target for defect-free stamp is 90% [44], Based on Murphy's model [45], a defect requirement for  $10 \text{ mm} \times 10 \text{ mm}$  stamp is  $\leq 0.1 \text{ defects cm}^{-2}$  [43]. This is a much tighter spec than that of the EPI wafer used for lighting applications. Aixtron demonstrated  $\sim 0.1 \text{ defects cm}^{-2}$ , corresponding to yield to  $>90\%$  in  $10 \text{ mm} \times 10 \text{ mm}$  stamp by utilizing *in-situ*  $\text{Cl}_2$  cleaning process and cassette-to-cassette automation [42]. For different applications, the specifications of defects in the epitaxial wafer are different. For example, the defect size is  $1 \mu\text{m}$  for a  $5.8'' 2560 \times 1440$  resolution (QHD) smartphone, while the defect size is around  $3 \mu\text{m}$  for  $55'' 3840 \times 2160$  resolution 4K TV [46].

The third category is limited by material properties and physical properties, including the FWHM of the emission spectrum and the wavelength stability as a function of the current density and temperature, which are difficult to improve. The color gamut requirements for displays are getting tighter, and REC 2020 becomes the new standard. Display industries have used various standards in the past decades. Typical ones are standard Red Green Blue (sRGB), Digital Cinema Initiatives P3 (DCI-P3), and Recommendation 2020 (REC 2020). sRGB is an RGB color space that HP and Microsoft created to use on monitors in 1996 and standardized by

the International Electrotechnical Commission. DCI-P3 is an HDR RGB color space introduced by the Society of Motion Picture and Television Engineers in 2007. Ultra-high-definition (UHD) Alliance announced their UHD-TV specifications, which requires devices to displays at least 90% of the DCI-P3 color space. International Telecommunication Union Recommendation BT.2020, namely REC 2020, defines UHD-TV aspects, including a wide color gamut. For CIE 1931 color space, the REC 2020 color space covers 75.8%, compared to 53.6% covered by DCI-P3, and only 35.9% covered by sRGB.

For 100% coverage of the REC 2020, a narrow FWHM  $<20 \text{ nm}$  is required, or at least better than the competitors, OLED and LCD. The FWHM of LCDs with QD ( $20 \sim 30 \text{ nm}$ ) backlight is much narrower than those of OLEDs [47], corresponding to a color gamut of approximately 90% REC 2020. Typical FWHMs of InGaN blue, InGaN green, InGaN red, and AlInGaP red are 18 nm, 30 nm, 50 nm, and 20 nm. Due to the strong indium segregation effect in the InGaN MQWs, it is difficult to reduce the FWHMs of InGaN green and red microLEDs. Due to the strong polarization field in the MQW, the blueshift with increasing current density is another big issue of InGaN RGB microLEDs. This issue may be solved by pulse width modulation (PWM) by CMOS driver control. Some GaN-based LEDs grown with particular technologies also show very narrow FWHM and stable wavelength with applied currents, such as rare earth doping, but they are still under development.

## 2.2. Effect of various substrates on InGaN LED

The InGaN blue and green LEDs are grown on pattern sapphire substrate (PSS), which can significantly reduce the threading dislocation density (TDD) in the GaN epilayer and enhance light extraction efficiency (LEE) compared to that on the conventional single side polished sapphire (SSP) [48]. However, PSS does not work for high PPI microLED application because the mainstream dry-etch PSS pitch is  $3 \mu\text{m}$ , and wet-etch PSS is  $3.5 \mu\text{m}$ . The PSS cannot enhance light extraction efficiency when the microLED size is similar or smaller than the PSS pitch size. The PSS pattern can even diffract the light pattern of the microLED and make image uniformity worse. SSP or nano-scale PSS (NPSS) needs to be used in high PPI microLED applications. NPSS is claimed to reduce TDD and enhance the LEE more efficiently than conventional PSS [49, 50] because of the relaxed lattice mismatch and thermal mismatches between NPSS and GaN epilayer.

Another solution to improve the wavelength uniformity, enhance efficiency, and reduce the droop is to grow GaN-based LED on semipolar or nonpolar GaN free-standing substrates. The polarization-induced internal field in the MQWs can be absent or mitigated when GaN grows along with these directions [51]. Therefore, the wavelength stability and efficiency droop for nonpolar and semipolar LEDs have been improved considerably, desirable for microLED applications [52, 53].

Although the unique challenges to grow GaN-on-Si, Si is another desirable choice as a substrate. There are several advantages to use Si as a substrate to grow GaN-based

microLEDs. The most important one is the low cost, and the available commercial Si substrates are up to 12''. In contrast, SiC and Sapphire substrates are typically 4'' or 6''. Moreover, the monolithic integration used to make microLED display in AR/VR/MR applications needs to bond an LED wafer with Si CMOS backplane. The big difference of thermal mismatch between the sapphire substrates of the microLED and the Si backplane makes accurate control of microLED in bonding difficult. The thermal mismatch leads to at least 2.1  $\mu\text{m}$  misalignment when applying Au<sub>0.8</sub>Sn<sub>0.2</sub> bonding at 280 °C [54]. This issue can be avoided by using Si as a substrate for InGaN microLEDs growth. Another advantage of using the Si substrate is that removing Si via the wet-etching method is much easier than removing sapphire substrates by laser lift-off (LLO). Recently, Jiang's group demonstrated record EQE of orange and red InGaN LEDs on Si substrates [55]. They believe the significant tensile strain in InGaN-on-Si enhances Indium incorporation efficiency and helps grow long-wavelength InGaN LED [55]. Plessey announced InGaN red LED on Si substrates. Allos also partners with KAUST to develop high-efficiency InGaN red microLED on Silicon.

### 2.3. Technologies to achieve high EQE AllInGaN red LED

In the past 10 years, the improvement of InGaN long-wavelength LED performance is tremendous. The well-known 'green gap' is almost covered. Osram achieved high-efficiency green InGaN LED with a record efficacy of 209 lumens per watt (lm W<sup>-1</sup>) at a wavelength of 540 nm. The corresponding EQE is 58% at 540 nm. Jiang's group achieved record high-efficiency InGaN yellow and red LEDs with a peak WPE of 42.8% at 1 A/cm<sup>2</sup> with a wavelength of 577 nm and a peak WPE of 24.0% at 0.8 A/cm<sup>2</sup> with a wavelength of 608 nm, respectively [55]. Glö demonstrated the ability to manufacture blue, green, amber, and red LEDs based on InGaN NW and planar structures [56]. These results shed light on developing high-efficiency InGaN red LED. We will review the challenges and solutions for manufacturing high-efficient long-wavelength InGaN LEDs in the next section.

There are three main reasons which make the growth of long-wavelength LEDs with high-indium-content difficult. The first one is the large lattice mismatch (11%) between InN and GaN, causing significant strains and high TTD. The second problem is the strong quantum-confined Stark effect (QCSE) in the high-In composition InGaN MQW. QCSE spatially separates the electron and hole wave functions in QWs, which leads to low radiative recombination and low internal quantum efficiency (IQE). The third issue is the poor crystal quality of the InGaN layer with high indium composition. Owing to the low dissociation temperature of InN (~600 °C), high indium content InGaN needs to be grown at low temperature [57]. Low growth temperature and high strain lead to a high density of several types of defects, including V defects, stacking faults, misfit defects, and rough interfaces due to insufficient surface migration of atoms. These defects act as non-radiation centers, resulting in a low radiative recombination rate. Besides, the cracking efficiency of ammonia reduces dramatically under 600 °C [58]. When the indium

composition in InGaN is high, phase separation of InGaN material and even indium droplets is easily induced. Facing the above three problems, solutions to improve long-wavelength LED performance can be divided into three categories. The first method uses special substrates, templates, nanostructures, and epi structures to release strain. The second solution is to employ the bandgap engineering to suppress QCSE and improve IQE. The third approach is to optimize growth conditions to improve the InGaN MQW crystal quality. Substrates, templates, bandgap engineering, and nanostructure InGaN red LED will be reviewed in the following sections.

#### 2.3.1. Growth on various substrates to release the strain.

Due to the significant lattice mismatch between GaN and InN, people use InGaN template or unique substrates and structures to release the strain in high indium content InGaN QW materials. Soitec has developed an 150 nm thick relaxed InGaN pseudo-substrate (InGaNOS) [59]. Soitec demonstrates the importance and necessity of the InGaN substrate for high In-content InGaN MQWs growth by using three types of InGaNOS with various lattice parameters of 3.190 Å, 3.200 Å, and 3.205 Å [60]. Figure 2 displays the photoluminescence (PL) spectra of the In<sub>x</sub>Ga<sub>1-x</sub>N/In<sub>y</sub>Ga<sub>1-y</sub>N MQWs grown on the three InGaNOS substrates. The emission wavelength of the MQW grown on the GaN template is 447 nm, whereas that of the MQWs grown on 3.190 Å locates at 483 nm, i.e. a redshift of 36 nm by increasing template lattice parameter of 0.2%. The MQWs grown on InGaNOS of 3.200 and 3.205 Å emit at 507 and 509 nm, respectively, with the same MQWs growth conditions. Figures 2(b) and (c) are InGaN MQWs grown at different conditions to increase Indium composition on three InGaNOS substrates.

The lattice constant of ScAlMgO<sub>4</sub> is 0.3249 nm, leading to a lattice match with In<sub>0.17</sub>Ga<sub>0.83</sub>N and a 1.8% lattice mismatch with GaN. Ozaki demonstrated In<sub>x</sub>Ga<sub>1-x</sub>N/In<sub>y</sub>Ga<sub>1-y</sub>N MQWs ( $x > 0.2$ ,  $y \sim 0.17$ ) red LED on lattice-matched In<sub>y</sub>Ga<sub>1-y</sub>N templates on (0001) ScAlMgO<sub>4</sub> [61]. The critical thickness of high indium composition InGaN on the In<sub>0.17</sub>Ga<sub>0.83</sub>N template is much higher than that on the GaN template. Figure 3 compares the temperature dependencies of the integrated PL intensities of the In<sub>x</sub>Ga<sub>1-x</sub>N/In<sub>y</sub>Ga<sub>1-y</sub>N QW emitting at ~625 nm on both ScAlMgO<sub>4</sub> and sapphire. The PL intensity ratios between low temperature and room temperature are 13.6% for the QW on ScAlMgO<sub>4</sub> and 0.35% for the that on sapphire, suggesting that the former provides a 40-fold improvement of IQE [61]. The peak wavelength of In<sub>x</sub>Ga<sub>1-x</sub>N QWs on sapphire blueshift with the excitation intensity increase due to the state-filling and screen of QCSE, while the wavelength of the In<sub>x</sub>Ga<sub>1-x</sub>N/In<sub>y</sub>Ga<sub>1-y</sub>N QW on ScAlMgO<sub>4</sub> is almost independent of the excitation intensity shown in figure 4 [61]. This behavior is crucial for the microLED display application.

#### 2.3.2. Improve EQE by bandgap engineering.

Bandgap engineering is one of the main approaches to design the EPI structure. Yoshikawa *et al* proposed a structure of InN/GaN MQW consisting of one monolayer (ML) and fractional

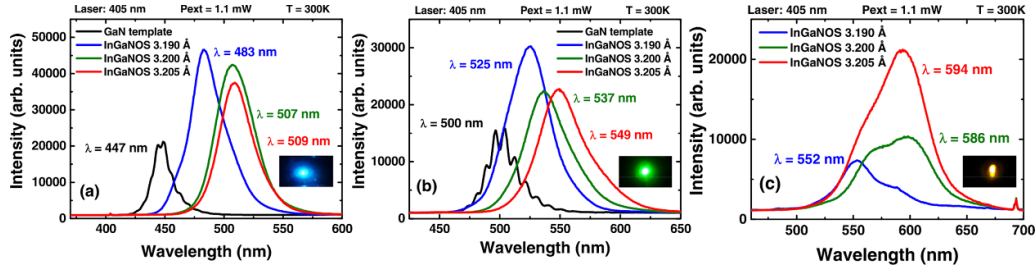


**Figure 2.** PL spectra of three InGaN heterostructures grown on three InGaNOS with a different lattice constant (the blue curve is related to InGaNOS 3.190 Å, green curve to 3.200 Å, red curve to 3.205 Å, and black curve to the reference GaN template). Insets: Pictures of PL emission. Reprinted from [60], with the permission of AIP Publishing.

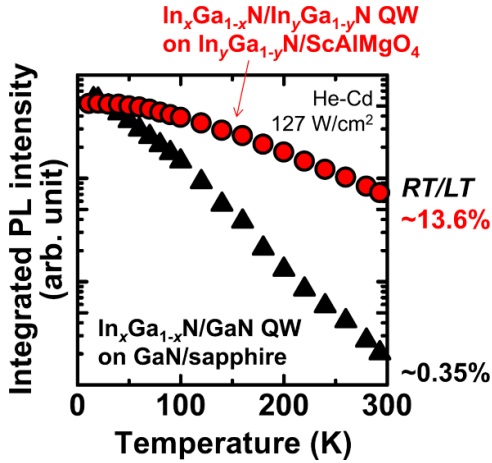


**Figure 3.** Temperature dependence of the PL intensities of the ~25 nm QW on ScAlMgO<sub>4</sub> and sapphire. Reproduced from [61]. © IOP Publishing Ltd. All rights reserved.

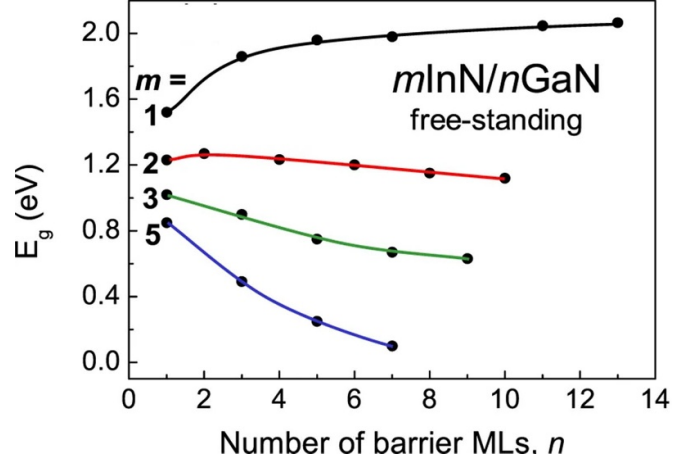


**Figure 5.** Calculated band gaps of mInN/nGaN SLs vs. number of barriers MLs. Reprinted by permission from Springer Nature Customer Service Centre GmbH: Scientific Reports [63] (2017).

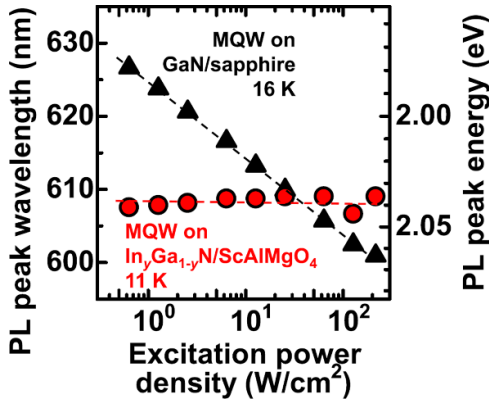


**Figure 4.** Excitation intensity dependence of PL peak of the QW on ScAlMgO<sub>4</sub> and sapphire at 11 and 16K. Reproduced from [61]. © IOP Publishing Ltd. All rights reserved.

ML InN QW insertion in the GaN matrix to realize long-wavelength emission [62]. Based on this idea, Gorczyca *et al* simulated red and even longer wavelength LED structures by using first-principles calculation of the electronic band structure [63]. In figure 5, the calculated band gaps versus layer thicknesses for sets of mInN/nGaN superlattice (SL) are presented in a free-standing strain mode. One ML InN/12 ML GaN SL can generate red emission based on their calculation.

The critical thickness of the InN epilayer on GaN is about 1 ML [64]. Thus, these MQWs are theoretically free of misfit dislocations. Moreover, the crystal quality of one ML InN-on-GaN can be improved by higher growth temperatures because each N atom is bonded to one In atom and three other Ga atoms. The abrupt interface between InN and GaN can be obtained and confirmed by XRD due to the self-atomic-ordering effect [62, 65].

An alternative approach to get red emission from GaN by bandgap engineering is doping GaN with rare-earth (RE) ions. The active layer of the device shown in figure 6(a) is 100 loops of 10 nm thick GaN and 3 nm thick GaN: Eu layers, which are grown at a temperature of 960 °C and using EuCp<sup>pm</sup>2 as the Eu source [66]. The GaN: Eu LED has an output power of 1.25 mW at 20 mA, and a peak EQE of 9.2% [67], which is the highest reported EQE for a GaN-based red LED. The inset of figure 6(b) indicates the emissions at two different applied currents. The emission wavelengths of these LEDs are centered at 621 nm, with an FWHM of 1 nm. The two emissions have nearly the same spectral shape. As a result, it maintains its ‘atom-like’ properties at different excitation intensity, resulting in an emission wavelength-independent to applied current and temperature [67]. These two characteristics are beneficial in microLED display applications.

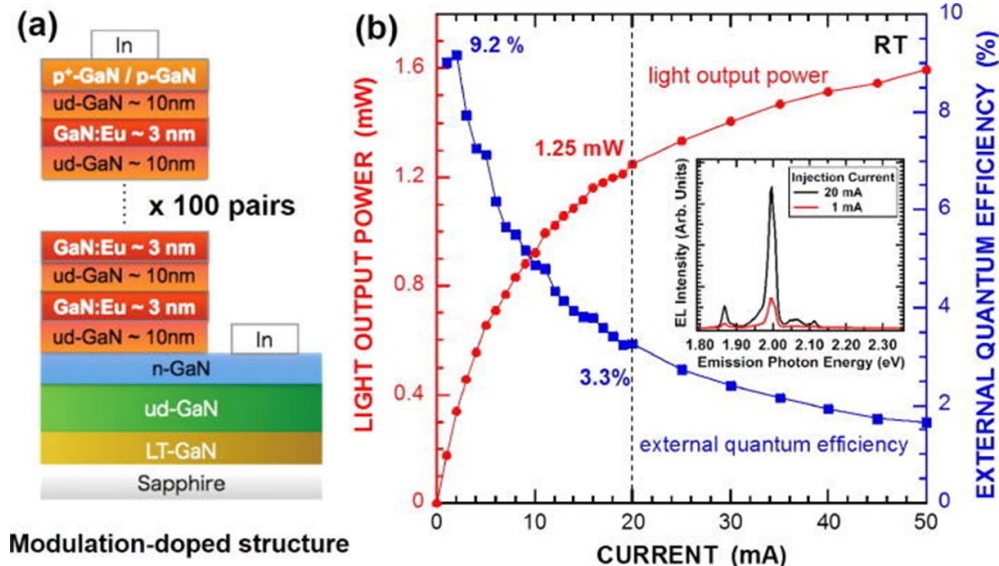


**Figure 6.** (a) Schematic of an LED with an active layer comprised of 100 pairs of alternating GaN and GaN: Eu layers. (b) The output power and EQE from this LED as a function of injection current. Reprinted from [67], with the permission of AIP Publishing.

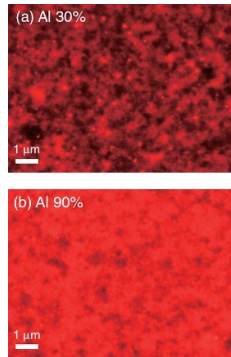


**Figure 7.** Fluorescence of red LEDs with AlGaN IL of (a) 30% and (b) 90% Al contents. Reproduced from [70]. © IOP Publishing Ltd. All rights reserved.

A 1–2 nm thick AlGaN insert-layer (IL) between InGaN QW and GaN QB is proved to be an effective method to improve EQE of the green and red LED due to increased electron and hole overlap. Toshiba's team proposed and implemented this method to achieve excellent green and red LED [68, 69].  $Al_{0.3}Ga_{0.7}N$  and  $Al_{0.9}Ga_{0.1}N$  are the optimized structure for green and red LEDs, respectively. For red LED, the fluorescence images of the dotted emission using  $Al_{0.3}Ga_{0.7}N$  and the more uniform emission using  $Al_{0.9}Ga_{0.1}N$  are shown in figures 7(a) and (b), respectively [70]. The red MQW is a 3 nm thick InGaN QW layer and a 10 nm thick InGaN barrier layer, with a 1 nm thick AlGaN IL between them. The Indium compositions of the QW and QB layers are around 35% and <1%, respectively [70]. The light output power ( $P_{out}$ ) and EQE at 20 mA were 1.1 mW and 2.9% at 620 nm in figure 8.

### 2.3.3. Nanostructure red LED growth.

InGaN/GaN nanostructure LEDs are fully or partially strained due to their

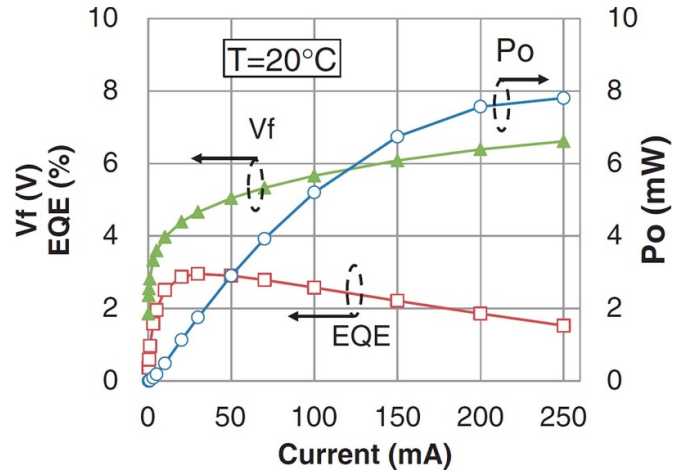


**Figure 8.**  $P_{out}$ , EQE, and  $V_f$  properties vs. applied current. Reproduced from [70]. © IOP Publishing Ltd. All rights reserved.

size, resulting in a low dislocation density [71–73]. Thus, they are expected to contribute to making high-efficiency InGaN LED due to less non-radiative recombination rate. Furthermore, there are no sidewall defects caused by mesa etching because the sidewall is formed during epitaxial growth, which is the key to improve microLED EQE. Finally, the emission wavelength of III-nitride based NW can be controlled by tuning the diameter and pitch of the NW [74].

Based on the emission color control scheme, Glō demonstrated InGaN-based NW LEDs with full visible color emissions shown in figure 9 [56]. First, a NW core is grown from an opening on the GaN template. Then the growth conditions are adjusted to enhance the radial growth of the rest parts of the LED structure, including the InGaN MQW and a p-type stack. The growth conditions strongly affect the NW size and

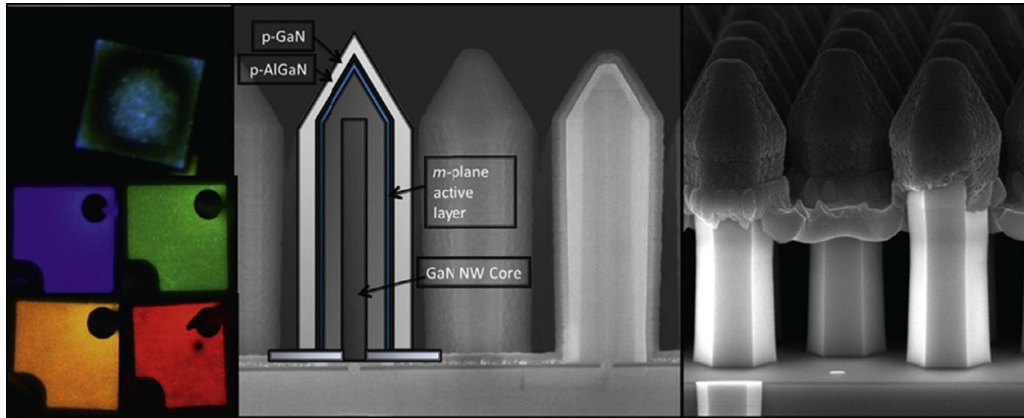


**Figure 9.** Left above: EL from the RYGB NW-LEDs fabricated by Glō AB, Lund. Center frame: side-view SEM image showing nanowire LEDs monolithically grown on a GaN-on-Si wafer in Lund. The edge of the top contact layer is visible. Right: air-bridge process. Reprinted from [56], Copyright (2016), with permission from Elsevier.

shape; therefore, growth condition optimization must obtain the uniform hexagonal NW arrays shown in figure 9 [56]. The processing of NW-LED is entirely different from those of the planar LED due to the very different geometries. An NW microLED contains numerous NW-LEDs contacted in parallel. The p-contact layer can be made on top of the NWs.

Aledia, a spin-off from CEA-LETI, and other groups also demonstrated red emission based on different nanostructure LEDs. Aledia has developed a 3D architecture microLED using GaN-on-silicon NW combining the color conversion method [75]. The panel fabrication consisted of three steps: the growth of blue NW-LED over a silicon substrate, color conversion, connection with a CMOS driver.

### 3. MicroLED chip characteristics and fabrication

#### 3.1. RGB microLED chip structures

There are three chip structures in broad-area LED, namely lateral chip, flip-chip, and vertical chip. The choice of chip structure must consider the matching and interacting all process steps in the entire technological chain from microLED manufacturing to application. Some examples are shown below. The most widely used and developed lateral chip structure in lighting application has not been applied to microLEDs because only vertical chip and flip-chip can be bonded on the backplane. The flip-chip structure must be used for fluidic transfer. It is better to use vertical chips in AR and VR applications because of the high PPI requirement. For AlInGaN microLED, a vertical structure is used because the absorbing GaAs substrate is removed. Plessey uses all InGaN RGB vertical microLED for panel manufacturing because their InGaN LEDs are grown on Si substrates that must be removed.

The comparison between flip-chip and vertical chip microLED, flip-chip microLED can be utilized for <1000 PPI applications, and the vertical chip can be used for >1000 PPI applications because of a bigger effective active region. As the chip size shrinks, the cost of manufacturing flip-chip is higher than the vertical chip due to more process steps. Since the n and p pads in flip-chip are smaller for the same chip

size than a vertical chip, equipment requirements to make flip-chip are higher. However, it is simpler to process flip-chip InGaN LEDs by avoiding the complicated substrate LLO process. Moreover, it is easier for the bonding process because the n and p pads in flip-chip can be connected mechanically and electrically in one step.

In broad-area LED, the EQEs of the best flip-chip and the best vertical chip InGaN are similar. However, a simulation shows that the efficiency of microLED arrays with sapphire is 61% higher than that without substrate [76]. The angular color variation of microLED displays with the sapphire substrate also can be reduced by almost 73%. The substrate increases the possibility of emitting photons into the air through additional diffraction or reflection, thereby improving LEE. When a substrate thickness is <20  $\mu\text{m}$ , the emitting efficiency increases significantly as the substrate thickness increases, shown in figure 10 [76]. When the thickness is >20  $\mu\text{m}$ , the efficiency rises slowly as the substrate thickness increase and reaches the maximum efficiency at the substrate thickness of 90  $\mu\text{m}$ . The color variation calculation follows the CIE 1931 and Information Display Measurement Standard. The simulation results in figure 11 show that the color variation of a microLED array with the substrate is less than that without substrate. In 90  $\mu\text{m}$  thick substrate chips, the  $\Delta u'v'$  at a broad view angle can be reduced by 0.012, which is a huge improvement. Experimental results show good consistency with simulation substrate [76].

However, the sapphire substrate causes significant optical crosstalk problems in microLED displays. The Depth-resolved confocal emission images indicate that the transparent sapphire substrate acts as an optical waveguide, resulting in crosstalk and poor signal-to-noise ratio [77]. Li *et al* also show that the intensity beyond the pixel (crosstalk effect) becomes dozens of times lower when the sapphire substrate is removed or Si is used to replace the sapphire substrate [77, 78]. Also, when multiple microLED pixels are illuminated simultaneously, the crosstalk effect is more pronounced. Compared with a single microLED pixel, the noise peak intensities of dual and triple microLED pixels increased by 58% and 100%, respectively [78].

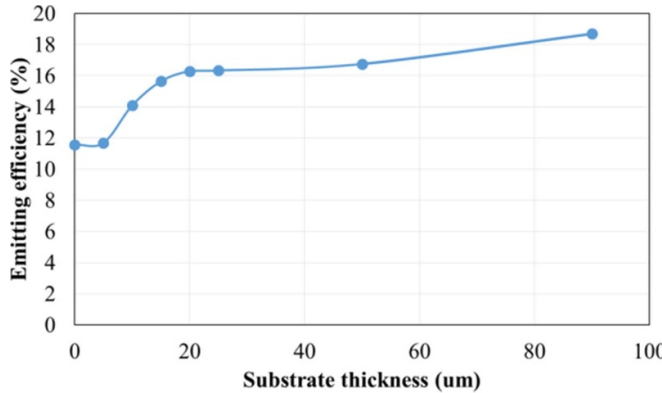


**Figure 10.** Substrate thickness vs. emitting efficiency. [76] John Wiley & Sons. Copyright © 2019 WILEY-VCH Verlag GmbH & Co. KGaA, Weinheim.

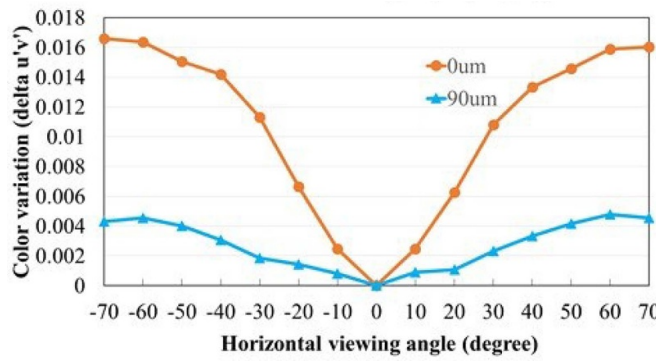


**Figure 11.** Comparison of color variation for microLED without or with a 90  $\mu\text{m}$  thick substrate. [76] John Wiley & Sons. Copyright © 2019 WILEY-VCH Verlag GmbH & Co. KGaA, Weinheim.

**3.1.1. Red AlInGaP and RGB InGaN vertical chip structure and process flow.** A typical structure and process flow of the AlInGaP red vertical microLED display panel is described below in figure 12 [79] to represent a typical vertical chip case (a) ITO and reflector metal deposition for the p-layer, (b) sapphire bonding, (c) GaAs substrate removed by grinding and wet etching, (d) AuGe/Au deposition, (e) epilayer etching, (f) ITO isolation, (g) metal deposition, (h) polymer flattening, (i) metal deposition, and (j) a side view of the display structure. Many teams choose vertical InGaN LEDs for blue and green to match AlInGaP red vertical chips. The above process flow also represents the process flow of InGaN vertical RGB microLED display, except for the different materials and process conditions. The sapphire substrate is removed by an LLO process for InGaN LEDs-on-sapphire. The Si substrate is removed by mechanical grinding and chemical etching processes for LEDs-on-Si. The metal for n and p contacts and pads are also different in III-nitride LEDs.

**3.1.2. InGaN flip-chip structure and process flow.** The schematic side view diagram of a typical flip-chip InGaN microLED bonding to sub-mount is shown in figure 13 [80]. The sub-mount can be PCB, Si MOS IC, or LTPS. The flip-chip InGaN microLED is made by a similar process for

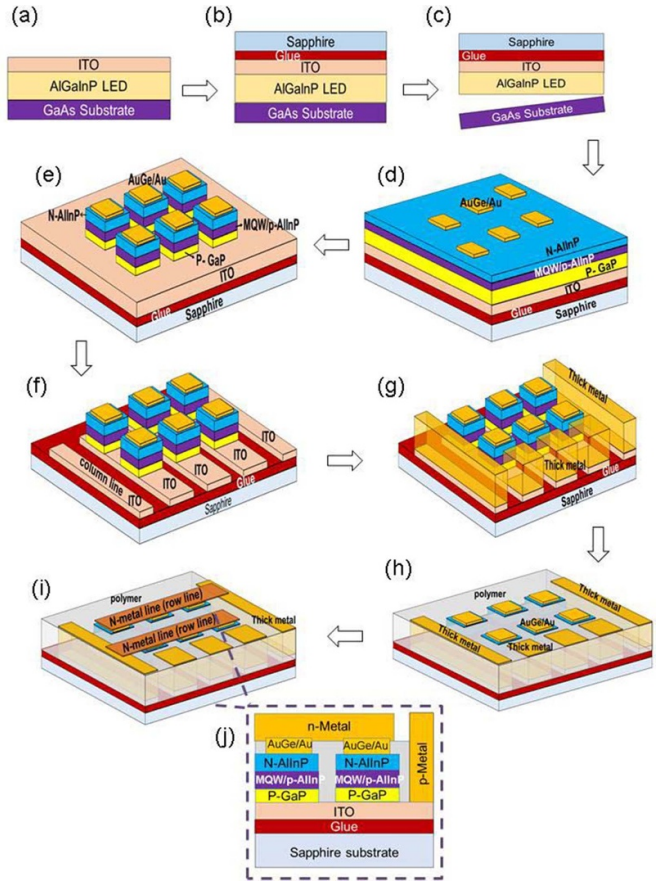


**Figure 12.** The typical process flow of the AlInGaP vertical microLED display panel. © (2018) IEEE. Reprinted, with permission, from [79].

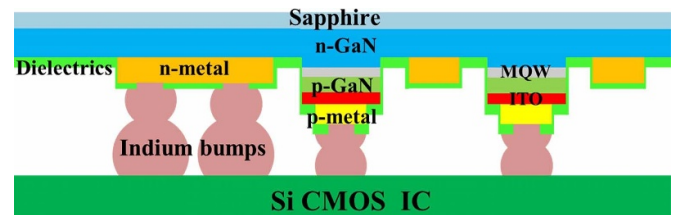


**Figure 13.** Cross-section of the flip-chip microLED array connecting with a CMOS driver. © (2019) IEEE. Reprinted, with permission, from [80].

flip-chip broad-area LEDs, but a shrunk device size with the following typical processes (a) ITO, Ni or Ni/Au layer deposition as transparent contacts for p contact, (b) Al or Ag reflector deposition by e-beam, (c) pixel definition and formation by ICP-RIE, (e) Ti/Al deposition as the common cathode, (f) SiO<sub>2</sub> or SiN passivation layer deposition by plasma-enhanced chemical vapor deposition (PECVD) or atomic layer deposition (ALD), (g) Indium or Au bumps deposited on the metal electrode, (h) microLED array is bonded onto a CMOS driver. The images display through the sapphire substrate because the flip-chip microLEDs are bottom light emitter.

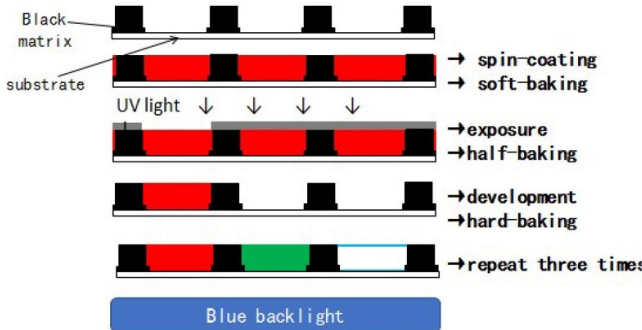


**Figure 14.** The typical structure and process flow of the quantum-dot color-conversion panel. [83] John Wiley & Sons. Copyright © 2019 WILEY-VCH Verlag GmbH & Co. KGaA, Weinheim.

**3.1.3. Color conversion RGB chip structure and process flow.** The RGB microLEDs also can be achieved by color conversion from blue/UV flip-chip or vertical chip microLED. This method is much simpler than RGB direct emission technologies because only one color microLED is used. The same structure and characteristics of three RGB chips also make the system design simpler. However, it still suffers from color crosstalk, low efficiency, short LT, and so on. New phosphor, solvent materials, structures, and processes have been developed to solve these problems [81, 82]. Color conversion RGB can be mainly realized by three methods. Figure 14 shows the conventional structure and process flow of QDCC panel fabrication. (a) red QDs and photoresist (QD-PR) coating on the substrate having black matrixes, (b) soft baking, (c) patterning by aligner, (d) QD-PR removal and hard baking, (f) repeat the same process for green and blue QD-PR [83]. Colloidal QDs are usually utilized as the color conversion materials due to small size, tuneability of color, high quantum yield, and low cost. They are usually synthesized by the chemical solution process. Propylene glycol methyl ether acetate is widely used as the solvents for QDs because it is the same solvent for PR. Therefore, it is easier to be incorporated into a well-developed photolithography process. If UV light is chosen as the excitation light for higher optical density, a UV blocking matrix and blue QDs are needed.

Another method is first to make a patterned QDCC film and then pattern the film on the surface of the blue/UV microLEDs. This method is promising because it has been widely used in SSL to make broad-area white LEDs from blue LEDs. RGB QD in PR solutions and the film behave differently, compared by Kim *et al* [84]. When microLEDs are smaller than 5  $\mu\text{m}$ , the film needs to be thin to avoid lateral loss and crosstalk. The absorption of the QD film needs to be high enough to minimize blue leakage and enhance the red/green emission; thus, a high QDs concentration is required.

The third promising method is inkjet printing, which is a well-developed manufacturing process in the display industry. Prof. Kuo's group utilized this approach to obtain full-color microLED displays by using the aerosol jet (AJ) technique for the first time in 2015 [85]. Inkjet-printed InP/ZnS QD film is

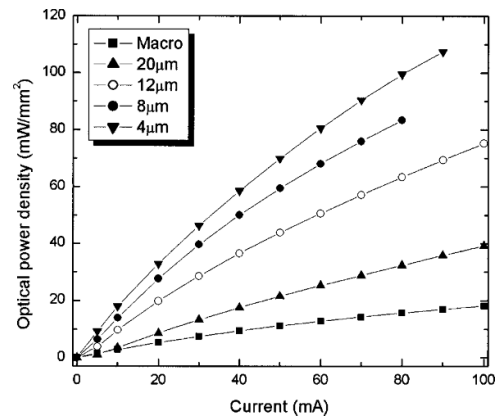


**Figure 15.** Optical output power as a function of current of microLEDs with different sizes. Reprinted from [89], with the permission of AIP Publishing.

also reported to absorb >95% of blue light when the thickness of the film is  $\sim 10 \mu\text{m}$  [86]. However, AJ printing works only when the microLED size is  $\geq 10 \mu\text{m}$ . A super-inkjet printing system to spray the QDs with a linewidth of 1.65  $\mu\text{m}$  was reported [87]. It is believed that ink printing can make color conversion film as small as to submicron.

### 3.2. Characteristics and theories of the microLED

All the microLEDs have similar behavior, no matter AlInGaN or AlInGaP, which is much different from broad-area LEDs. Their features, theories, challenges, and solutions are discussed in this section.

**3.2.1. Emission efficiency.** Researchers proposed micro LED decades ago to improve optical output power ( $P_{\text{out}}$ ). Dai *et al* demonstrated a two-fold higher  $P_{\text{out}}$  from 6  $\mu\text{m}$  microLED [88, 89]. Choi *et al* fabricated microLED from 4 to 20  $\mu\text{m}$  and found five times enhancement in  $P_{\text{out}}$  shown in figure 15 [89]. This increased  $P_{\text{out}}$ , compared to the broad-area LED, is an attribute to higher LEE because of light emitting from the sidewalls. Figure 16 shows the image of a 12  $\mu\text{m}$  microLED array under electron beam excitation [89]. A bright ring at the side of the microLED devices is observed, evidencing the sidewall emission enhanced. The higher LEE comes from not only more chance for photons to escape from the sidewall and periphery of the top surface but also the higher extraction from the titled sidewall discussed in section 3.3.2.

The higher  $P_{\text{out}}$  in microLEDs seems contrary to the lower microLED efficiency described in the overview section. If we use the current density ( $j$ ) as the  $x$ -axis and the EQEs as the  $y$ -axis to redraw the curve in figure 15, we will get EQE vs.  $j$  curve. This curve gives us some insights into the difference between microLEDs and broad-area LEDs. In the EQE vs.  $j$  curve, the peak EQE of smaller chips is lower, which tells us that the efficiency of microLEDs is lower than that of the broad-area LEDs. Therefore, EQE vs.  $j$  is widely used in microLEDs characteristics to replace the luminance/output power vs. current ( $L$ - $I$ ) curve in broad-area LED. Moreover, the current density is a more reasonable parameter than current

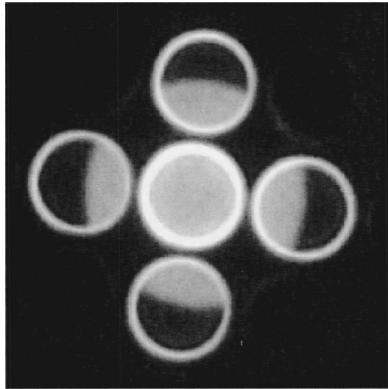


**Figure 16.** Image of 12  $\mu\text{m}$  microLED array under a 40  $\mu\text{m}$  wide electron beam excitation. Reprinted from [89], with the permission of AIP Publishing.

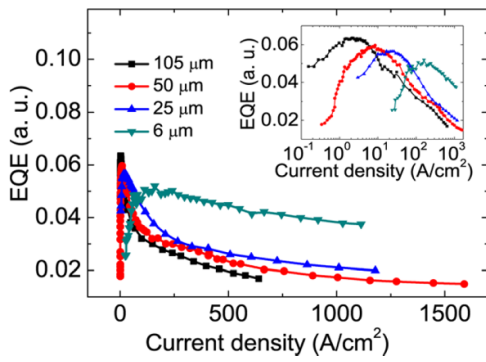


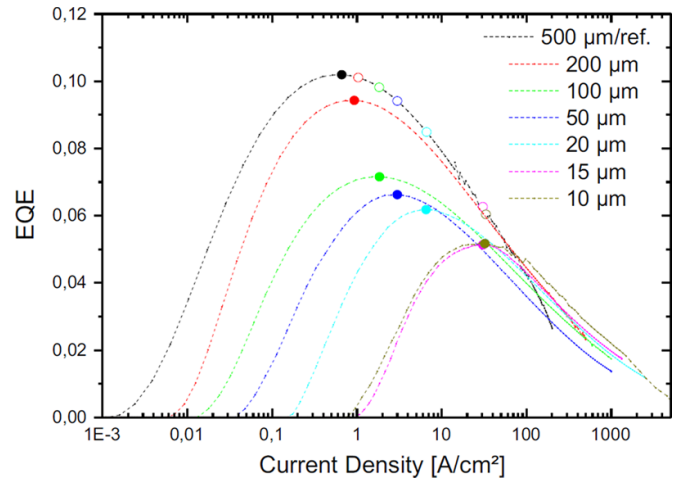
**Figure 17.** EQE vs.  $j$  for microLED with different sizes. Reprinted from [90], with the permission of AIP Publishing.

when comparing microLEDs with different sizes. Figures 17 and 18 show two typical EQEs vs.  $j$  curves for microLEDs with various sizes [90, 91]. Both experimental results show two trends in the EQE variation as the device dimensions shrank, the reduction of peak EQE and the higher current density where the peak EQE is. These two behaviors are the essential characteristics of current microLEDs, and the reduced peak EQE is the main problem in microLEDs that need to be solved.

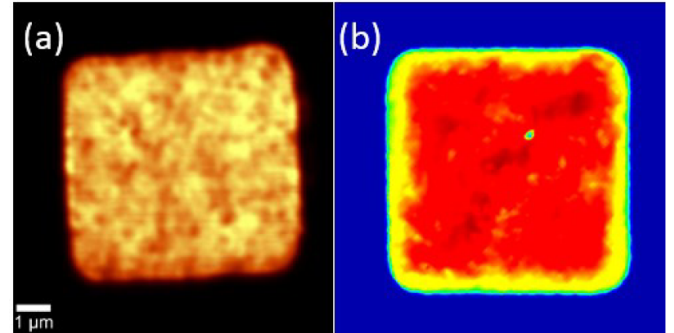
The lower peak EQE at higher  $j$  in microLED results from a higher sidewall defect density in a smaller chip that leads to an increased Shockley–Read–Hall (SRH) non-radiative recombination [90–92].

Figure 19 shows PL and cathodoluminescence (CL) images of two 7  $\mu\text{m}$  microLEDs [93]. Both PL and CL show that the emission intensity at the microLED edge area is degraded, with a width of around 800 nm. The emission intensity at the periphery of the devices should be higher due to higher LLO, similar to what is shown in figure 16. These results imply that the EQE reduction in small microLED can be attributed to increased non-radiative recombination in the sidewall and P-layer [93]. Some researchers believe that the non-radiative surface recombination occurs on the entire sidewall of the LED, including p-layer, MQW, and n-layer regions.

The ABC model used to analyze broad-area LED IQE also works well to microLEDs with various device dimensions



**Figure 18.** Experimental and simulated EQEs are shown in EQE vs.  $j$  curves. Reprinted from [91], Copyright (2017), with permission from Elsevier.



**Figure 19.** (a) Photoluminescence and (b) cathodoluminescence intensity maps at 440 nm of 7  $\mu\text{m}$  LEDs. [93] John Wiley & Sons. Copyright © 2017 WILEY-VCH Verlag GmbH & Co. KGaA, Weinheim.

[94]. The IQE of microLEDs can be expressed by a simple model [95].

$$\eta_{\text{IQE}} = \frac{\eta_i B n^2}{An + Bn^2 + Cn^3} \quad (1)$$

where  $n$  is carrier concentration. The maximum efficiency reach when  $d\eta_{\text{IQE}}/dn = 0$ , thus, the carrier concentration at maximum efficiency is [95]

$$n = \sqrt{A/C}. \quad (2)$$

When the defect-related coefficient  $A$  increases, the efficiency decrease, and the maximum EQE location moves to a higher  $n$ , or higher current density. Therefore, the higher sidewall defects related nonradiative recombination in microLED reduce IQE and EQE and move the EQE peak to a higher current density region.

The coefficient  $A$  increases around two orders with LED dimensions shrinking, shown in figure 20(a). The values of coefficient  $A$  also show a linear relationship to the perimeter/surface ratio, which suggests nonradiative recombination is related to LED sidewalls defects rather than defects

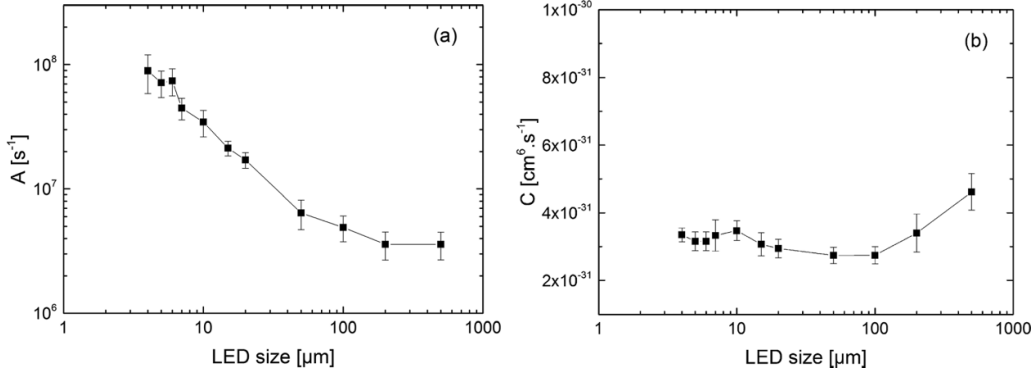


**Figure 20.** (a) Extracted coefficients  $A$  and  $C$  as a function of LED size. Coefficient  $A$  shows a stronger dependence on the LED size, while coefficient  $C$  is independent with chip size. Reprinted from [96], with the permission of AIP Publishing.

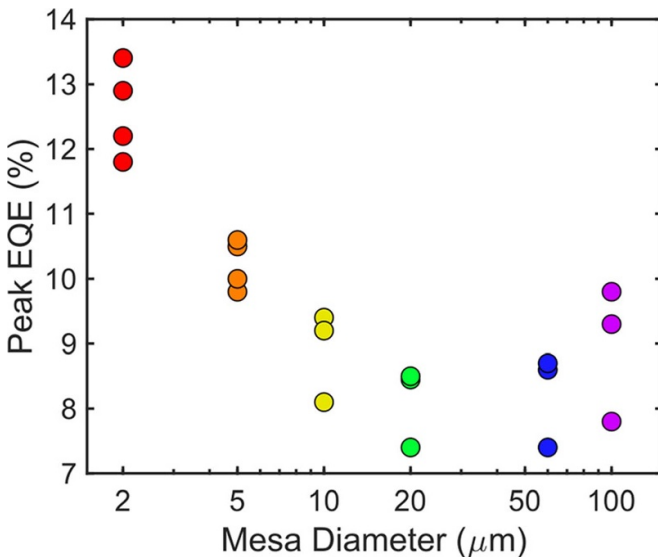


**Figure 21.** Maximum EQE for microLEDs with different sizes, whose sidewall defects are minimized. Reprinted from [97], with the permission of AIP Publishing.

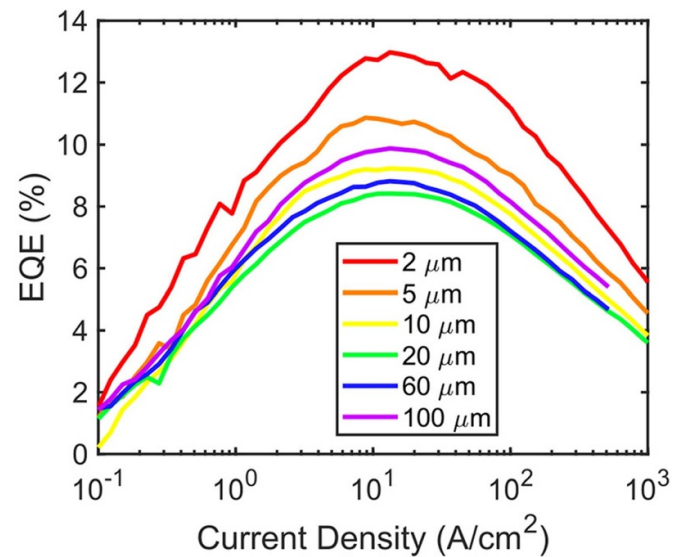


**Figure 22.** EQE curves for different size microLEDs. Reprinted from [97], with the permission of AIP Publishing.

inside [96]. Consequently, efforts must be undertaken to lower the sidewall defects that reduce microLED efficiency. These results also indicate that the efficiency droop is similar at high current densities, no matter what is the microLEDs size because of the almost unchanged coefficient  $C$  with chip size shown in figure 20(b) [96].

UCSB team reported that EQE increases as the size of the microLED decreases for the first time by minimizing the sidewall defect [97]. Maximum EQEs increase from  $\sim 9\%$  to  $\sim 13\%$  for microLED sizes reduce from  $100 \mu\text{m}$  to  $2 \mu\text{m}$ , shown in figure 21, which seems contrary to the results in figures 17 and 18. These trends are explained by increasing LEE on the sidewall in smaller chips verified by simulation, which is only observable when sidewall defects are minimized [97]. This explanation is consistent with the results reported by Choi [98]. The LEE of the microLEDs is the competition between the nonradiative recombination caused by sidewall defects and the enhanced extraction from sidewall shown in

figure 16. When the nonradiative recombination due to sidewall defects is lower than enhanced extraction from the sidewall, the higher EQE can be observed in smaller microLEDs. Furthermore, the peak EQE location and shape of EQE vs.  $j$  curves for all devices are similar, shown in figure 22, which indicates SRH nonradiative recombination is suppressed in small chips based on equation (2) [95].

One crucial observation from EQE vs.  $j$  curve in figures 17, 18, and 22 is that the EQE of microLEDs can exceed that of broad-area LEDs at high current densities. The phenomenon results from the different current crowding, thus the junction temperature. In smaller microLEDs, current spreading is better, avoiding the regions where the current localized and much higher than other areas. Auger recombination is much higher in the high current density area even the coefficient  $C$  is almost constant, resulting in an efficiency droop. Higher local carrier concentration in the bigger chip cause local overheating and then device degradation. Less strain possibly also helps the microLEDs, which have a larger height-to-width aspect ratio. The higher EQE at high current density in microLED is one

reason people use microLED for VCL applications that require high luminance.

**3.2.2. Current density voltage characteristics.** For the same reason,  $j$  vs. voltage ( $j$ - $V$ ) is characterized in microLED to replace the conventional current–voltage ( $I$ - $V$ ) curve in broad-area LED. A typical  $j$  as a function of the voltage curve is shown in figure 23 [90].  $J$ - $V$  curve of microLEDs shows a strong size dependence. The current density of smaller microLEDs is much higher than that of the large ones at the same current/voltage due to obvious reasons. For example, the  $j$  at 5 V of a 6  $\mu\text{m}$  LED is around six times higher than that of a 105  $\mu\text{m}$  LED in figure 23. The inset of figure 23 is the relationship between the logarithmic  $I$ - $V$  curve for microLED with different sizes. Higher forward leakage current in smaller microLED can be seen clearly on a logarithmic scale. In smaller microLED, lower EQE is usually associated with higher leakage current due to the higher mesa perimeter/surface ratio. This will give us a clue on how to improve EQE; that is, the methods to reduce leakage current are usually useful approaches to suppress sidewall defects and improve EQE.

**3.2.3. Angular radiation pattern and color shift.** Different from the Lambertian radiation pattern of red AlGaInP and blue/green AlGaInN broad-area LEDs, the far-field radiation patterns of the AlInGaN green/blue and AlInGaP red microLEDs are shown in figure 24 [99]. Both simulation and experimental results show that the light emission from the AlGaInP red chip is Lambertian. In contrast, the light intensity gets stronger from the normal angle to  $\sim 40^\circ$  and then decreases for InGaN based green and blue microLEDs.

The lights generated in the MQWs can be extracted from the top surface and four sidewalls of the chip. The sidewall/top surface emission ratio in AlInGaP microLED is much smaller than that in InGaN green and blue ones because of the much stronger absorption in red AlInGaP LED than that of green/blue InGaN LED. The emissions of RGB LEDs from top surfaces are all Lambertian. As the microLED shrinks, the sidewall emissions from all RGB microLEDs increase because of less internal absorption and reflection losses. The sidewall emission from InGaN green and blue chips are much stronger, resulting in different radiation patterns among AlGaInP red microLED and InGaN blue/green counterparts shown in figure 25. Furthermore, the color shift of RGB microLED displays becomes visually noticeable [99].

The different radiation patterns of InGaN broad-area LEDs and microLEDs mean more light emitting from the sidewall in microLEDs, which is evidenced in figure 16 [89]. Non-Lambertian distribution in InGaN microLED is one of the basic features of microLED, which means the light extraction efficiency increased by more light from the sidewall. Therefore, enhancing the light emitting from the sidewall is one crucial method to improve InGaN microLED EQE, which will be discussed in section 3.3.

**3.2.4. Temperature of microLED.** Figure 26 shows the simulation results of junction temperature vs.  $j$  for microLEDs

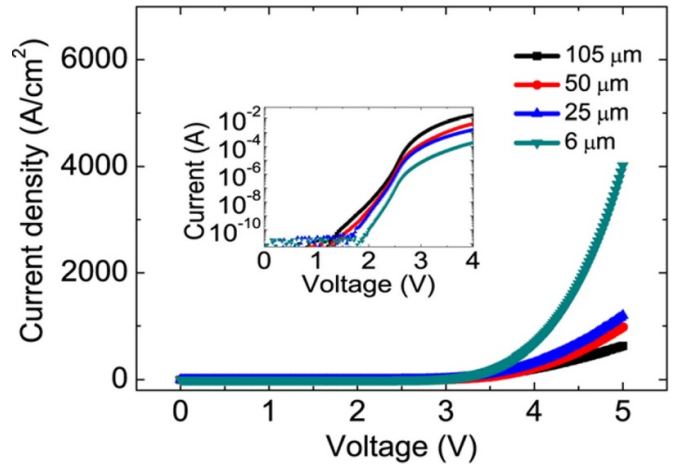


**Figure 23.** Current density vs. voltage of the microLEDs with different sizes (inset is current for comparison). Reprinted from [90], with the permission of AIP Publishing.

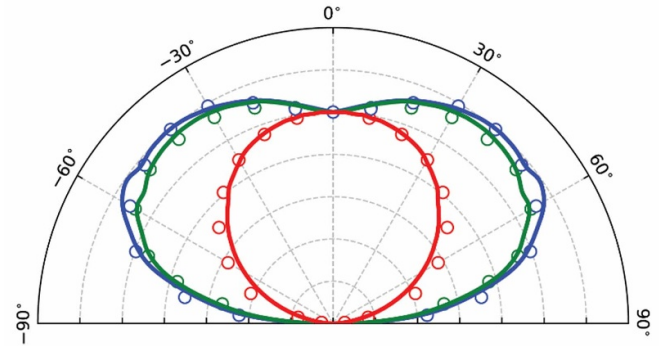


**Figure 24.** Experimental and simulated radiation patterns of AlInGaN green/blue LEDs (green/blue lines) and AlInGaP red microLEDs (red line). Reproduced from [99]. CC BY 4.0.

of different sizes [92]. Based on the simulated results, the junction temperature increases significantly with the chip size increase at a given current density. The current is localized close to the electrode due to current crowding, causing a similar distribution of the heat and temperature in the junction region. Due to the current crowding depending on the chip size, the specific thermal resistance increases with the microLED size increase, leading to stronger self-heating in larger microLEDs. The simulation is consistent with the reported results in near UV microLEDs [100].

**3.2.5. Size-dependent wavelength shift with current density.** A typical emission peak wavelength and FWHM of microLED as a function of injection current at the low current range are shown in figure 27 [80]. Peak wavelength blueshifts from 5 to 1000  $\mu\text{A}$  for an 8  $\mu\text{m}$  LED, a typical operating current density range for large displays. The blueshift results from the screen of QCSE and the band-filling effect. Simultaneously, the FWHM increases with the current increase from 5 to 1000  $\mu\text{A}$  due to the joule effect.

MicroLED for VLC application works at a much higher current density. The emission peak wavelength as a function

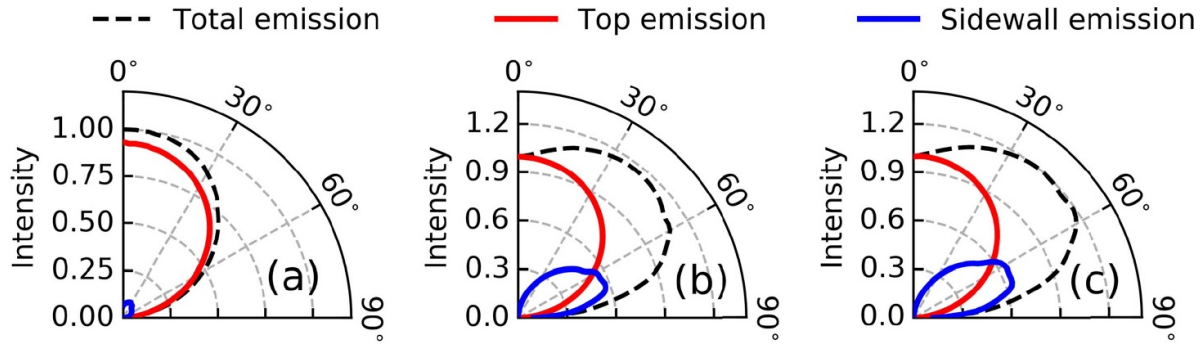


**Figure 25.** Simulated total, top, and sidewall emissions of (a) red, (b) green, and (C) blue microLEDs at different viewing angles. Reproduced from [99]. CC BY 4.0.

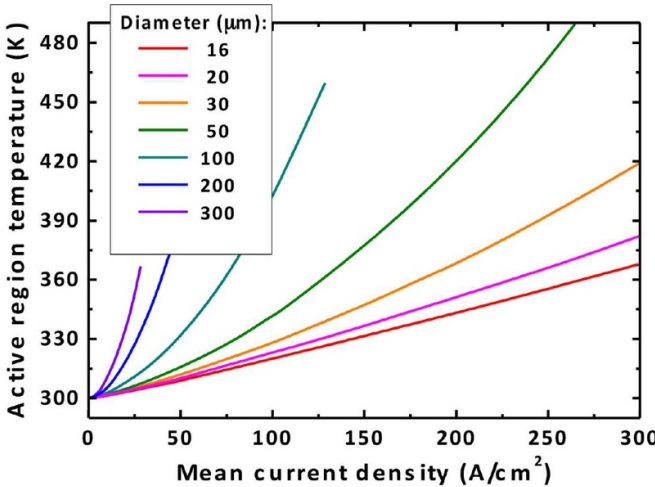


**Figure 26.** LED junction temperature vs.  $j$  for microLEDs with different size. [92] John Wiley & Sons. Copyright © 2017 WILEY-VCH Verlag GmbH & Co. KGaA, Weinheim.

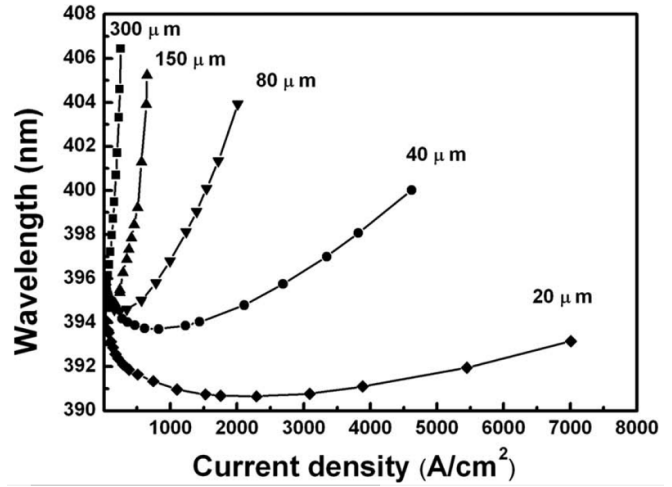


**Figure 28.** Wavelength as a function of current density in a wider range. Reprinted from [101], with the permission of AIP Publishing.

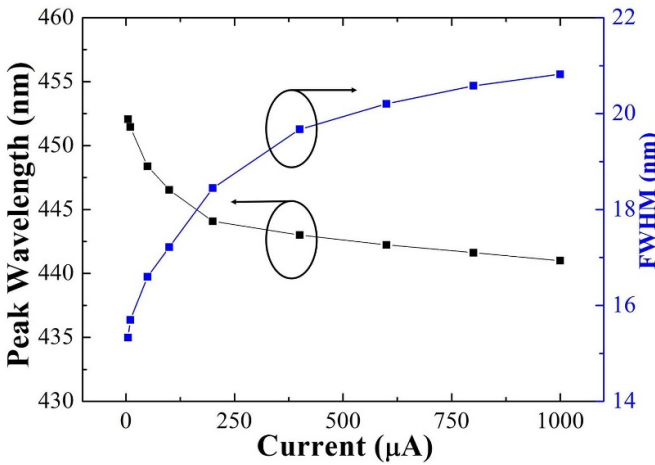


**Figure 27.** Wavelength and FWHM as a function of current for 8  $\mu\text{m}$  LED. © (2018) IEEE. Reprinted, with permission, from [80].

of the current density in a wider current density range for different chips is plotted in figure 28 [101]. In the higher current density region  $>1000 \text{ A cm}^{-2}$ , wavelength redshift when

current density increases, opposite to the wavelength vs. current trend in figure 27, due to the bandgap shrinkage with junction temperature increase. In conclusion, the wavelength shift depends on both current and chip size, a competition among the QCSE, band filling, and bandgap shrinkage. Since the wavelength redshift is primarily related to the increase of the junction temperature, it is reasonable for small pixels to have a lower junction temperature at the same current density, consistent with the conclusion about junction temperature of microLED in the previous section.

**3.2.6. Reliability of microLED.** MicroLED size has a significant impact on LED LT. VLC Applications required extremely high current density and brightness, which also impact LED reliability. The much lower junction temperature due to much better current spreading in microLED results in much better reliability than broad-area LEDs [102, 103].

Normalized light  $P_{\text{out}}$  as a function of operation time in microLEDs with sizes of 20, 40, and 60  $\mu\text{m}$  at the high operating  $j$  of  $3.5 \text{ kA cm}^{-2}$  is shown in figure 29. The  $P_{\text{out}}$  increases for a while (the first stage) and then falls (the second stage) [11]. The improved p-layer conductivity causes this behavior

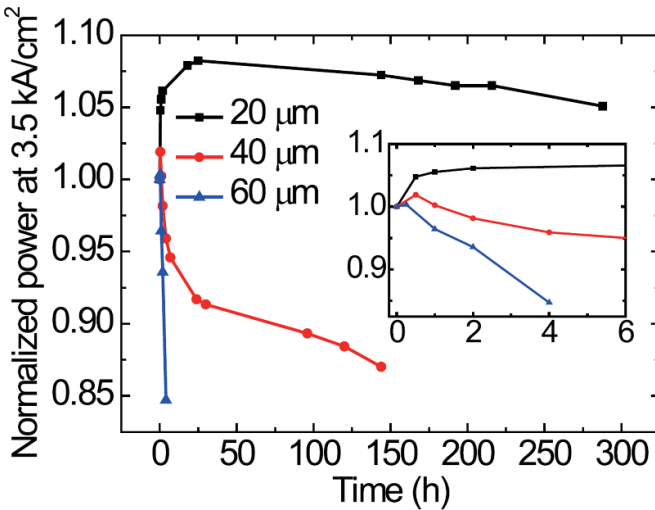


**Figure 29.** Normalized light  $P_{\text{out}}$  vs. operation time of microLEDs with various sizes. The inset is the  $P_{\text{out}}$  in the first 6 h. Reproduced from [11]. © IOP Publishing Ltd. All rights reserved.

due to more activated Mg in GaN under high junction temperature and high current flow [104, 105]. The power increase period of the 20  $\mu\text{m}$  chip is two orders longer than that of the 60  $\mu\text{m}$  one.

EQE reduction in the second stage is contributed to the stresses by injected carriers and high junction temperatures, which cause the defects and contact degradation [104, 106]. The EQEs of smaller microLEDs decrease less as the operating time increases, which results from better heat dissipation and lower junction temperature in smaller microLED, described in the previous sections. As a result, microLED has much better reliability than a broad-area LED.

The  $I$ - $V$  characteristics at different operation times of the 20  $\mu\text{m}$  microLED are shown in linear and semi-logarithmic scale in figures 30(a) and (b) [11]. The resistance has a fast reduction from 0 to 0.5 h and then decreases from 0.5 to 25 h, which agrees with the  $P_{\text{out}}$  quick/slow increase time frame in figure 29. The 40 and 60  $\mu\text{m}$  chips have similar behavior but a shorter time. The reduced power at the second stage is also consistent with the  $I$ - $V$  curve change in figure 30(b). In comparison, 40  $\mu\text{m}$  microLED has a higher leakage current than 20  $\mu\text{m}$  microLED, which reveals more defects generated during degradation in larger chip [107, 108]. Consequently, larger microLEDs develop defects faster, resulting in faster power degradation, worse reliability, and a shorter power increasing period. Again, these data verify a strong correlation among EQE, defects density, and leakage current in microLEDs.

### 3.3. Technologies to improve microLED EQE

Non-radiation recombination caused by sidewall defects from dry etching plasma-induced damage is the primary issue to be solved to improve microLEDs performance. Many techniques have been proposed and developed to solve this problem and thereby improve microLED EQE. On one side, mesa etching must be performed carefully to minimize sidewall defects.

On the other hand, the sidewall defects can be suppressed in different ways, such as annealing, passivation, wet etching, etc.

**3.3.1. Suppress the sidewall defects.** Tian *et al* improved the EQE of 6  $\mu\text{m}$  GaN blue microLED from 5% to 10% by increasing the thermal anneal time from 2 to 3 min after the mesa etch. Longer annealing time can recover the sidewall damages caused by mesa etching. EQEs in microLED at low current density has been recovered, but longer annealing has not changed its EQEs at high current densities region. These results also confirmed the effect of sidewall defects in tiny microLED [90].

Yang *et al* studied and optimized the wet etching and annealing process systematically to remove sidewall damage in GaN-based LED [109]. Figure 31 shows the  $I$ - $V$  curves of a perforated LED with annealing and  $(\text{NH}_4)_2\text{S}$  etching. Both the forward and reverse leakage currents are recovered after the optimized annealing and  $(\text{NH}_4)_2\text{S}$  wet etching treatment. The leakage current reduces to a level as low as the broad-area LED, suggesting the removal or passivation of all the sidewall defects. As mentioned previously, the reduced leakage current is usually associated with EQE improvement. Therefore, the annealing and wet etching have a chance to improve microLED EQE by removing the etching damages.

Passivation is an excellent method to passivate the dangling bond and defects caused by dry etching. UCSB reported a high-efficiency III-nitride microLED by sidewall passivation using ALD. The passivation layer deposited by ALD improves EQE compared with the one by PECVD. The peak EQEs of 20  $\mu\text{m}$  microLEDs with and without ALD sidewall passivation are 33% and 24%, respectively [110]. Several other groups also reported that the ALD is a better way to deposit the passivation layer since ALD has the advantages of excellent uniformity, high-quality film density, atom level thickness controllability, and perfect surface coverage [111].

UCSB group also demonstrated that EQEs improve 50%–60% when the microLEDs size shrinks from 20  $\mu\text{m}$  to 2  $\mu\text{m}$  for the first time by minimizing the nonradiative sidewall defects [97]. KOH wet chemical wet etching and  $\text{Al}_2\text{O}_3$  dielectric passivation are approved as an effective approach to minimize the sidewall defects dramatically in their work [97]. No leakage currents were seen in current density vs. voltage characteristics, confirming that leakage current is associated with sidewall defects and EQE reduction described in section 3.2.2 and Yang's experimental results [109].

Zhu *et al* suppressed the size-dependent efficiency drop in microLEDs by using ultralow-damage neutral beam etching (NBE) [112]. NBE is a low-defect etching technique for semiconductor materials, developed by Samukawa *et al* [113, 114]. The neutral beam suppresses the charged particles and ultraviolet photon radiation, exposing the substrate only to energy controlled neutral beam. When chip size is reduced from 40  $\mu\text{m}$  to 6  $\mu\text{m}$ , at a current density of 5  $\text{A cm}^{-2}$ , the EQEs of microLEDs etched with NBE and ICP decreases by <10% and 80%, respectively. These results verify that the root reason for

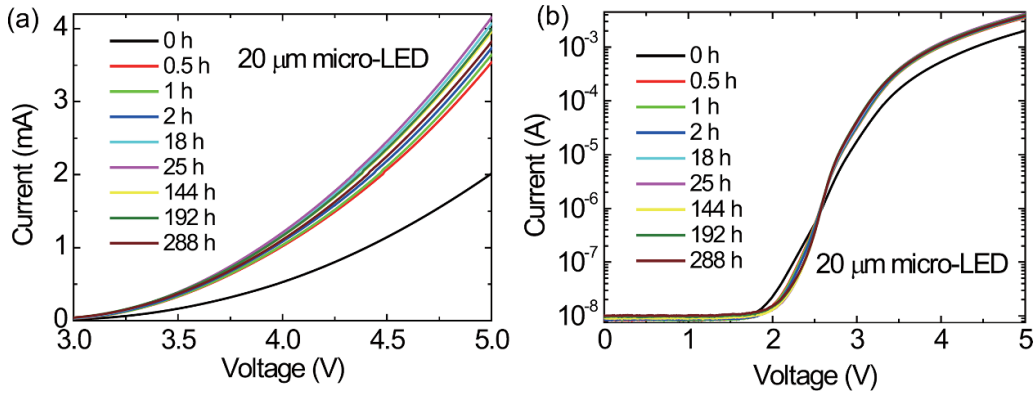


**Figure 30.** The  $I$ - $V$  curves of a  $20\ \mu\text{m}$  microLED at different operation times in (a) linear scale and (b) semi-logarithmic scale. Reproduced from [11]. © IOP Publishing Ltd. All rights reserved.

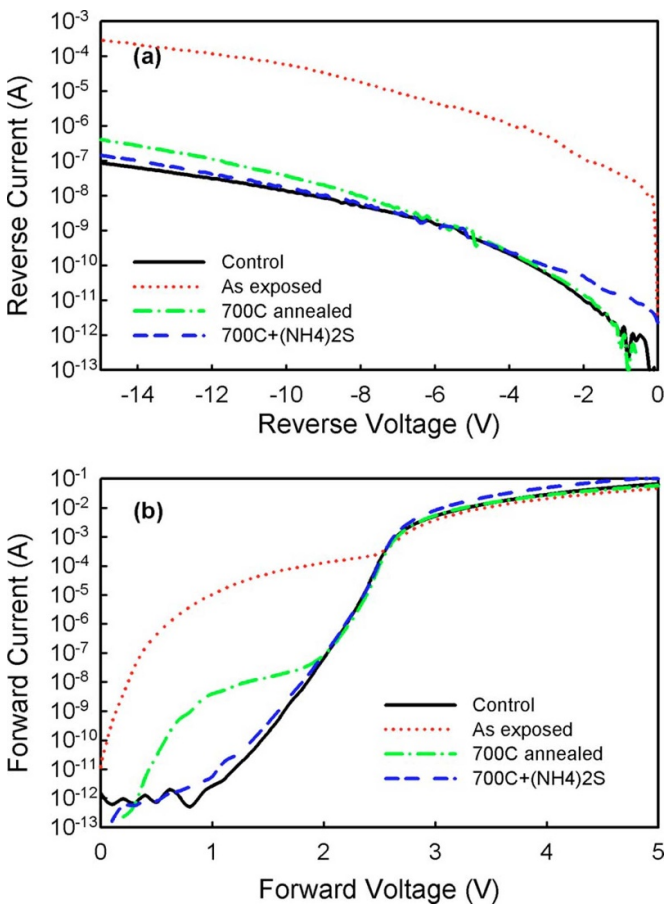


**Figure 31.**  $I$ - $V$  curves of perforated LEDs after annealing and  $(\text{NH}_4)_2\text{S}$  etching. Reprinted from [109], with the permission of AIP Publishing.

the microLED size-dependent EQE reduction is the etching-defects and show that the NBE is a promising technique to fabricate high-efficiency GaN microLEDs  $<20\ \mu\text{m}$ .

Sidewall defects cause low EQE in both AlGaInP and InGaN microLEDs. Ga-Frenkel and vacancy-interstitial defects are found on the surface of the GaP layer [115]. Zn diffusion into III-V compound semiconductor has been reported to compensate for the defects by several groups [116, 117].

Lee *et al* utilized post-Zn diffusion to suppress surface defects and improve the efficiency of the AlGaInP red 630 nm LED [118]. The  $P_{\text{out}}$  is enhanced from 7.4 mW to 11 mW, and the forward voltage is reduced by post-Zn diffusion. The improvement is assigned to reduce the surface defects on the Zn diffused window layer. This technology is also used in AlInGaP red microLED to passivate the sidewall defects. However, this technology is hard to be used in tiny microLED with a size of  $\leqslant 5\ \mu\text{m}$ .

**3.3.2. Reflector and chip shape to improve extraction efficiency.** Anis Daami *et al* reported a higher EQE by two main improvements. First, the etching process during mesa formation has been changed into a softer plasma. The second optimization is to replace the p metal from a nickel-based alloy with silver for better ohmic contact and higher reflectivity. Maximum EQE of  $7\ \mu\text{m}$  microLED increases from 4.8% to 6.8% by using these two technical improvements shown in figure 32. More importantly, the efficiency droop is highly reduced [93, 119]. The maximum EQE location increases from  $10\ \text{A cm}^{-2}$  to  $100\ \text{A cm}^{-2}$ , which implies that the EQE improvement is a result of the enhanced light extraction efficiency, not a higher IQE, based on the discussion of the equation (2) in section 3.2.1.

Yang *et al* reported that the  $\text{SiO}_2/\text{Al}_2\text{O}_3$  double dielectric passivation layer improves  $P_{\text{out}}$  of the LED. The first  $\text{Al}_2\text{O}_3$  layer effectively passivates the surface, and the second  $\text{SiO}_2$  layer with a lower index increases the critical angle of the extracted light. Also, the Fresnel reflection also enhances the  $P_{\text{out}}$  of LED with a double dielectric passivation layer. At the same time, the leakage current of the LED with the  $\text{Al}_2\text{O}_3$  passivation layer is at least 2 orders of magnitude lower compared to that of passivated with  $\text{SiO}_2$  layer and that without passivation. The reduced leakage currents confirm that the  $\text{Al}_2\text{O}_3$  layer passivates the damaged surface during dry etching and reduces nonradiative recombination on the surface. The LEDs  $P_{\text{out}}$  improved around 25% by using the  $\text{SiO}_2/\text{Al}_2\text{O}_3$  double passivation layer [111]. These methods and results are based on a broad-area LED, but they should work for microLED. The refractive index and the thickness of a dielectric layer can be

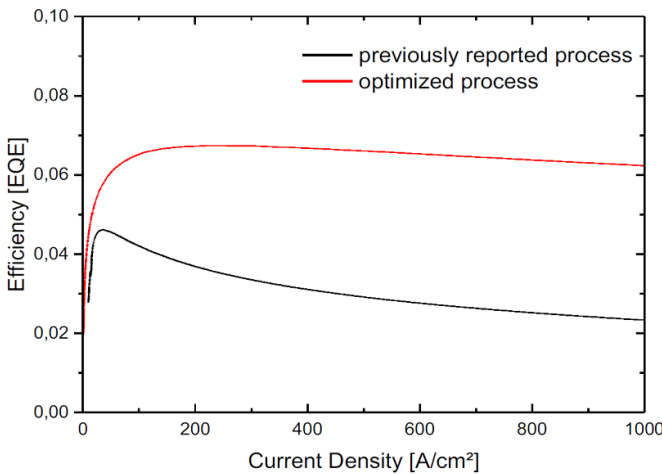


**Figure 32.** EQE as a function of current density. [93] John Wiley & Sons. Copyright © 2017 WILEY-VCH Verlag GmbH & Co. KGaA, Weinheim.

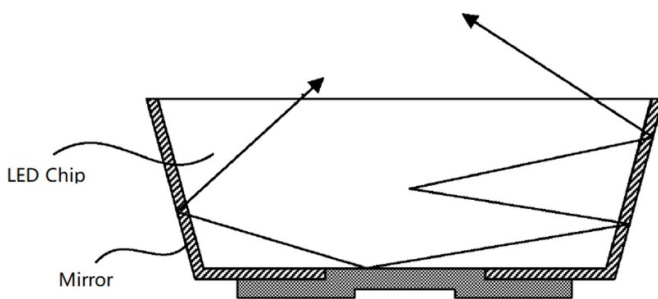


**Figure 33.** A microLED schematic with a sidewall mirror [120].

designed based on the Fresnel reflection for the anti-reflection in the following equations.

$$\text{Refractive index : } n_{\text{AR}} = \sqrt{n_s + n_A} \quad (3)$$

$$\text{Thickness} = \frac{\lambda}{4} = \frac{\lambda_0}{4n_{\text{AR}}} \quad (4)$$

Apple applied one patent of microLED with a dielectric side mirror shown in figure 33 [120]. The dielectric mirror is spanning along the lateral sidewall of the p-n diode and directly underneath the p-n diode. The dielectric mirror may include pairs of dielectric layers with different refractive indexes, including but not limited to  $\text{Al}_2\text{O}_3$ ,  $\text{MgF}_2$ ,  $\text{MgO}$ , and  $\text{CaF}_2$  [120]. Each layer may have a thickness of a quarter of the peak emission wavelength of the p-n diode ( $\lambda/4$ ), divided by the refractive index of the dielectric layer ( $n$ ) decided by equations (3) and (4).

Based on the above discussion, enhancing the emission from sidewall is one of the main approaches to improve LEE and EQE. InfiniLED's microLED technology also uses a parabolic microLED structure for light collimation and light extraction. The simulation shows that reflector on the top and sloped sidewall improves the efficiency and control of the light-emitting angle, as shown in figure 34 [121].

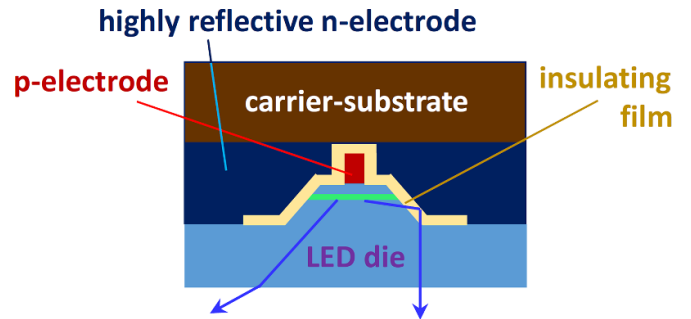


**Figure 34.** A microLED schematic with reflective sidewalls and shapes to collimate the light and enhance extraction. Reproduced from [121]. CC BY 4.0.

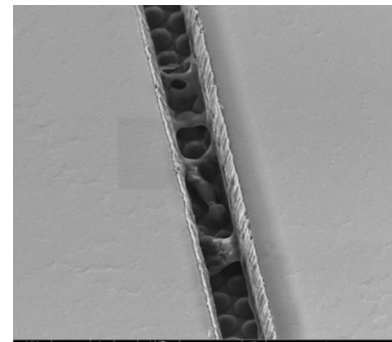


**Figure 35.** SEM image of photoresist residues in a narrow gap ( $6 \mu\text{m}$ ) between two nearby GaN LEDs. Reproduced from [122]. CC BY 4.0.

**3.3.3. Yield and uniformity improvement.** The yield and the uniformity of electrical/optical performances in the array are essential factors for displays. An etching to the sapphire substrate is required to isolate the subpixel. Xie *et al* have found that the gap between microLED has a significant impact on the yield and uniformity of microLED array [122].

With a  $170 \mu\text{m}$  gap between the mesas, the yield of microLED subpixels in the panel is around 90%, but the yield falls to about 67% with a  $6 \mu\text{m}$  wide gap. The reason for the low yield is the incomplete removal of the PR residue shown in figure 35. These PR residues cause the subsequent deposited  $\text{SiO}_2$  layer to degrade, resulting in a short circuit of the microLEDs. The issue is resolved by replacing solvent-based PR stripping with an  $\text{O}_2$ -based plasma ashing. This low-damage plasma treatment is known to be effective in completely removing PR residues. By adding an ashing step, the yield of the arrays with a  $6 \mu\text{m}$  gap increases from 67% to over 95%. The  $P_{\text{out}}$  variation of the array reduces from 18.1% to 6.4%. The author also found that the voltage variation is decreased by increasing the Ti/Au metal stack thickness [122].

#### 4. Mass transfer

RGB monochromatic microLED subpixels need to be accurately assembled at the designed location on the panel to achieve full-color displays. Transferring thousands of

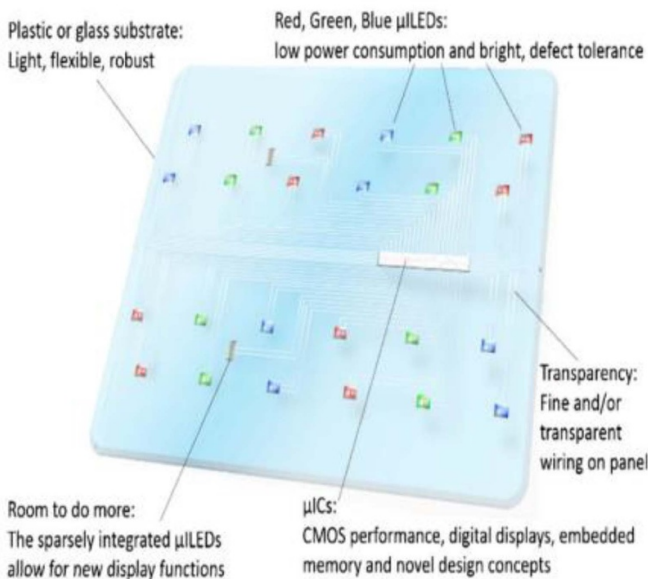


**Figure 36.** Illustration of a conceptual low PPI microLED display. Reproduced from [125]. CC BY 4.0.

microLEDs and bonding them with their drivers are tremendous technical obstacles since the process relies critically on transfer rate, alignment accuracy, bonding strength, and reliability. It takes the current transfer equipment and processes for more than 2 months to produce a 4K TV because around 25 million microLED chips need to be transferred [123]. The realization of such a display requires mass transfer technology with alignment accuracy within  $\pm 0.5 \mu\text{m}$ , yield >99.9999%, and a transfer rate of millions of chips per second [124]. No such high-speed, high accurate, high-yield, and low-cost solution is available yet.

There are currently two major paths to realizing mass transfer, namely direct monolithic integration and indirect pick-and-place. The monolithic approach is to directly hybridize the microLED array on the driving circuit by die-to-wafer or wafer-to-wafer bonding. It is only suitable for high PPI applications with small display screens such as projector, AR, VR, and MR. In low PPI applications, such as TV and laptop screens with a large panel, pick-and-place technology is inevitable. The microLEDs must be relocated to a completely different position from a small source wafer to a large panel with very high yield, which cannot be done in the direct transfer. A part of a typical low PPI microLED panel is shown in figure 36 [125]. Each microLED is manufactured as a subpixel and transferred to a matrix backplane using a pick-and-place method.

Indirect pick-and-place technology is complicated, but it also brings many benefits. MicroLED subpixels occupy only a small portion of the panel shown in figure 36. Compared to the chip-to-wafer or wafer-to-wafer monolithic transfer, most of the panel area is blank, making transparent display and flexible display possible to be realized. The space between chips is large enough to interconnect electronic devices and implement new functions. Furthermore, the microLED chips in a small

wafer can cover a large area in the panel to reduce the cost. This approach also avoids brightness crosstalk and color crosstalk. Moreover, a 100% yield is only achievable by repairing from pick-up-place technology.

To solve the critical problems in pick-and-place, many companies and research groups have proposed different solutions, such as electrostatic force transfer head, elastomer stamp transfer printing, beam addressed laser lift-off release, fluidic transfer, all-in-one RGB MicroLEDs on CMOS associated with microtube, magnetic stamp, roll to plate transfer, and so on. The above transfer technologies will be reviewed in detail below.

#### 4.1. Electrostatic transfer head

LuxVue, which Apple acquired in 2014, demonstrated the use of electrostatic forces to transfer microLED chips. In figures 37(a) and (b) [126]. The microLED transfer head consists of a substrate, mesa structures, electrodes above the mesas, and a dielectric layer covering the electrode. The microLED transmission head can pick up the microLEDs from the substrate and release them onto the receiving substrate by applying a voltage on it.

A carrier substrate that is utilized to hold a microLED is heated to a temperature lower than the bonding metal's liquidus temperature, and the transfer head is heated to a temperature higher than the liquidus temperature of the bonding layer. When the microLED is brought into contact with the transfer head, heat from the transfer head is transferred into the bonding layer to melt the bonding layer. Corresponding to the MicroLED chip that needs to be transferred, the voltage selectively applied to the transfer head generates a grasping force between the transfer head and the microLED that picks up the microLED from the carrier substrate. When the chip is transferred to the specified position, a negative voltage is applied, and the transfer head releases the chip [127].

#### 4.2. Elastomer stamp transfer printing

X-celeprint uses this technology to transfer microLED chips from a carrier to a target through a stamp. Figures 38 and 39 [128, 129] show a typical process flow and cross-sectional structure of a transferable and printable microLED chip in this method. A microLED is formed on a sacrificial portion of the substrate, and the transferable microLEDs are released from the substrate and attached with a tether to anchor portions. The microLEDs are then transferred to the target surface, usually by a relatively low spatial density. The stamp is made of a compliant elastomer with a rigid glass backing. The stamp is transparent for easy optical alignment [130, 131]. The soft elastomeric stamp meets the chip and creates an adhesive force created by van der Waals interaction. Adhesion is rate sensitive. The adhesion will take the microLEDs from the carrier and stick them on the elastomeric stamp at high speed. The stamper contacts the target substrate and moves the microLEDs on it at low speed [129]. The wafer-level stamp can transfer 82 863  $75 \mu\text{m} \times 90 \mu\text{m}$  chips in a single print operation with a 99.99% yield and transfer microLEDs down to  $3 \mu\text{m}$ .

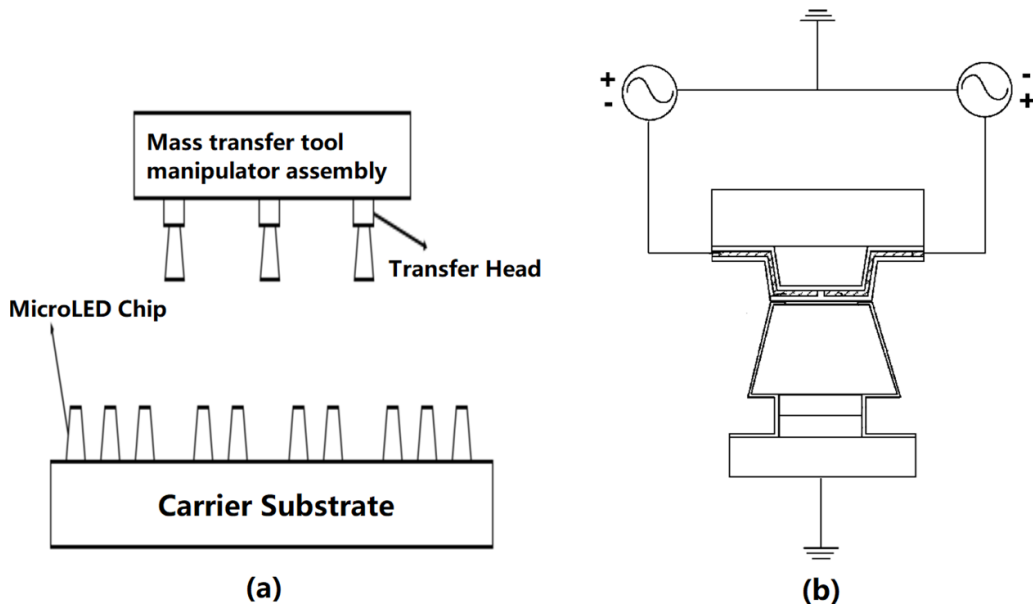


**Figure 37.** (a) Illustration of a transfer head array utilizing electrostatic force, (b) detailed structure of a transfer head [126].

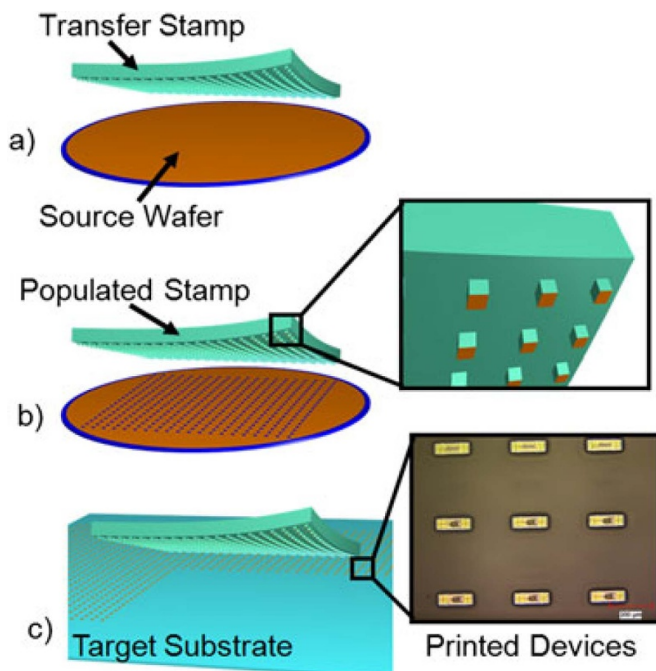


**Figure 38.** Process flow of elastomer stamp transfer printing. [128] John Wiley & Sons. Copyright © 2017 WILEY-VCH Verlag GmbH & Co. KGaA, Weinheim.

#### 4.3. Beam addressed laser lift-off release

Glō, Uniqarta, QMAT, and Tesoro Scientific claim a comprehensive approach, including new materials, new processes, and new test equipment [132–134]. The typical process flow is shown in figure 40. The process begins with transferring microLEDs grown on a substrate (Si, sapphire, SiC, GaAs) to a laser-transparent carrier coated with a sacrificial layer, namely a dynamic release layer (DRL). This transfer is performed that

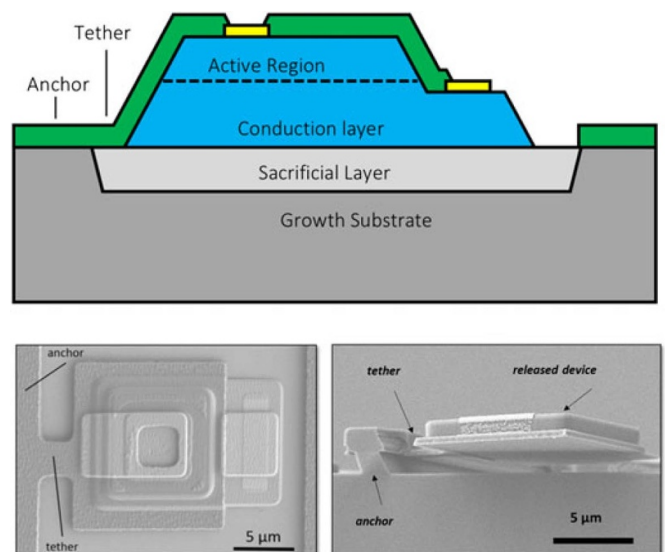


**Figure 39.** Schematic illustration, top and side view of a microLED prepared in elastomer stamp printing. [128] John Wiley & Sons. Copyright © 2017 WILEY-VCH Verlag GmbH & Co. KGaA, Weinheim.

the dies end up oriented on the DRL carrier active side away from the new substrate, ready for flip-chip assembly. Equally, the microLED can be transferred directly to the DRL carrier, in which case their active side will face the DRL for vertical chip transfer. In both cases, an LLO process releases the microLED from the source substrate. After the microLED is placed on the DRL, laser transmission is applied. During the laser transfer, a part of the DRL is ablated by a UV laser through the carrier substrate, thereby generating blisters in the DRL without breaking it. In addition to gravity, the expanded blister's force makes a transfer onto a receiving substrate [132, 133].

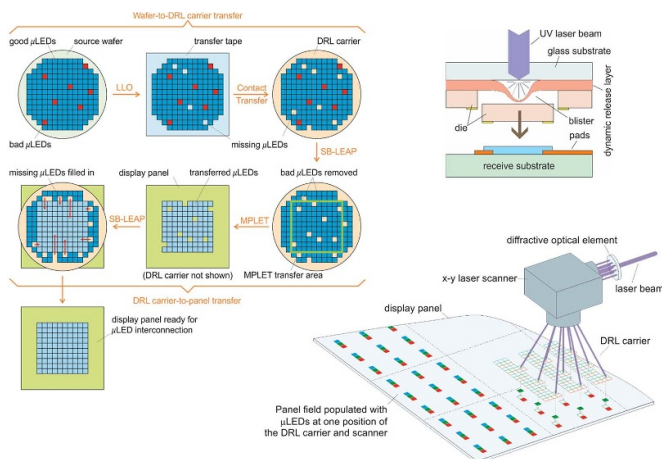


**Figure 40.** Process flow in know-good-die LLO release for microLED mass transfer. SB-LEAP is a single beam laser transfer process. [132] John Wiley & Sons. Copyright © 2018 WILEY-VCH Verlag GmbH & Co. KGaA, Weinheim.

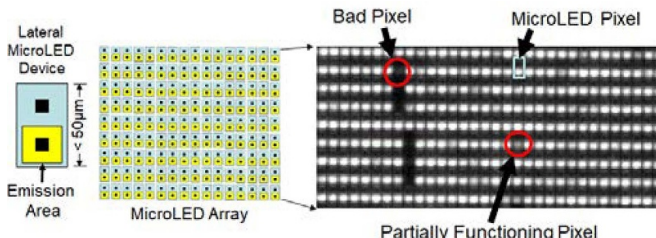


**Figure 41.** Contactless EL test of a microLED array. [135] John Wiley & Sons. Copyright © 2018 WILEY-VCH Verlag GmbH & Co. KGaA, Weinheim.

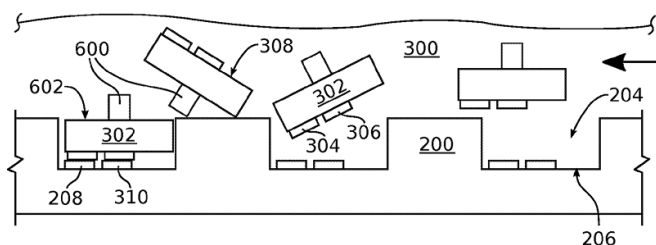


**Figure 42.** The schematic diagram of fluidic transfer [137].

MicroLED KGD functional test developed by Tesoro Scientific is a good plus and useful tool for industry [135]. Figure 41 shows an EL test mapping of a  $50 \mu\text{m}$  microLED array using a contactless EL test method. This EL test is a massively parallel, contactless EL method so that the throughput can be achieved in production, about 5 min for a 4" wafer test. This step is tested using a combination of PL and EL. After generating the KGD defect file, the microLED wafer and its KGD file are loaded into beam-addressed release (BAR) mass transfer equipment. Zero defect can be achieved by transferring KGD only. The BAR mass transfer method claims a high transfer rate of  $>100\text{--}250$  million KGD microLED chip per hour. For a 5" cellphone, the estimated assembly time is 1.5 min. Glō brought the microLEDs with substrates in contact

with the backplane. It has been prepared with bonding pads and eutectics of various heights for each RGB color [136]. The interconnection is achieved by an LLO process, which selectively detaches the die while the backplane is heated to melt the eutectic solder.

#### 4.4. Fluidic transfer

Sharp acquired eLux in 2017. Foxconn also invested in eLux to develop fluid transfer technology. eLux's fluid assembly technology uses carrier liquid to transfer microLED chips to the TFT backplane and assembles them in place for each pixel. The TFT backplane substrate has a top surface with wells. The bottom surface of each well has electrical connections. The liquid suspension of the microLEDs flows through the TFT backplane substrate, and the microLEDs are captured in the well shown in figure 42 [137]. As a result of annealing the TFT backplane substrate, an electrical connection is established between each microLED and the corresponding well. The eutectic solder interface metal on either the backplane or the microLED is desirable and the use of a fluxing agent before thermal annealing. The microLED can be a surface-mount LED with two electrical contacts on its top surface, adjacent to the wells' bottom surfaces. By using microPL and defect inspection during the chip process, this method will only collect good chips in the fluid. It takes 15 min to assemble a 12 inch microLED panel for both a 42 PPI display, including 518 400 LEDs, and a 168 PPI display, including 8294 400 LEDs. Besides, microLED chip orientation can be precisely controlled with a unique feature built on the chip. Since it is a self-alignment process, the Micro LED's pitch is not limited by the accuracy of transfer equipment. eLux has demonstrated the assembled microLED size as small as  $20 \mu\text{m}$ .

#### 4.5. Others

Many other transfer technologies are developed by utilizing various kinds of forces, summarized in table 4. Some examples are magnetic stamp and roller-to-plate print. The former technique proposed by Industrial Technology Research Institute (ITRI) is similar to electrostatic stamp transfer, but an electromagnetic force is utilized. Magnetic materials such as iron, cobalt, and nickel need to be mixed into the microLED to make it magnetic, making the process more complicated. A coil is used as the transfer head [124]. Roller-to-plate print is exhibited by the Korea Institute of Machinery & Materials (KIMM). The chips are transferred to the roller and then are imprinted on the target substrate by roller rotation [138]. This approach has a transfer rate of up to 10 000 chips per second with a chip size of  $<100 \mu\text{m}$ . However, it cannot selectively transfer microLED chips. It is also difficult to guarantee accuracy and reliability. CEA-LETI group proposed microtubes interconnections associated with all-in-one transfer [139, 140]. A basic unit consisting of all-in-one RGB MicroLEDs on CMOS driving circuit is fabricated and plugged on a display backplane using microtubes. Microtubes guarantee both mechanical and electrical interconnection. MicroLEDs are stacked directly on the

**Table 4.** Summary of mass transfer methods.

Transfer technology	Company	Force or method	Transfer rate
Electrostatic transfer head	LuxVue (Apple)	Electrostatic force	NA
Elastomer stamp transfer printing	X-celeprint	Van der Waals force	3 million h <sup>-1</sup>
Magnetic stamp	ITRI	Electromagnetic force	NA
Beam addressed laser Lift-off release	Glo, Uniqarta, QMAT	LLO and bonding	100–250 million h <sup>-1</sup>
Fluidic transfer	eLux	Gravity and capillary self-assembly	50 million h <sup>-1</sup>
Roller-to-plate transfer	KIMM	Imprinting	36 million h <sup>-1</sup>
Microtube	CEA-LETI	Mechanical force	NA

circuit. The connection is the shortest, which is essential in PWM mode. Moreover, it provides the best fill ratio, an ideal case for transparent displays, and high PPI displays.

## 5. Control circuit and panel

### 5.1. Control circuit designs

TFT are widely used as a backplane to drive display components, such as LCD, OLED, and microLED. MicroLED display contains millions of subpixels of red, green, or blue microLED chips, which are controlled by drivers. The driver can be amorphous silicon TFT ( $\alpha$ -Si TFT), LTPS TFT, or single crystalline silicon CMOS field-effect transistors. The control mode can be an active matrix (AM) or passive matrix (PM), current-drive, or voltage-drive. The PWM current drive method can achieve digital dimming by setting the current duty cycle [141]. Circuit design, mode selection, control mechanism, and techniques to build and improve panel performance are reviewed in this section.

**5.1.1. Active matrix vs. passive matrix.** AM or PM driving technologies are commonly used to drive microLED displays. Each row is activated in high-frequency order in both cases, and the pixels in the selected row are updated through the column data lines. Due to the persistence of vision, the human eye regards it as a planer frame rather than a line scan. In PM driving, the pixels in the remaining unselected rows are OFF and turn ON only for a short period when the row is chosen. In AM driving, they will remain active throughout the switching cycle until their values are updated again. This is the fundamental difference between PM and AM.

In PM, only one line can be selected and displayed simultaneously, so the display time of a single line will decrease as the number of lines increases, limiting the display size and resolution. In AM, on/off status and different gray levels of microLED can be independently controlled to avoid this problem. Moreover, a voltage applied to a selected pixel in PM mode inevitably affects the neighboring pixels and degrades the contrast of the display, i.e. crosstalk [142]. On the other hand, AM microLED (AMLED) has faster refresh rates and better brightness, which are suitable for high-performance video requirements. Overall, AM consumes less power than PM because its external circuitry consumes less energy, so they are efficient for large displays. Thus, AMLED is

more suitable to realize large-size, high-resolution, and high-performance displays, such as computer monitors, HDTVs, and billboards. More and more companies and research groups are working on AMLED.

**5.1.2. CMOS vs. LTPS.** The widely used drivers in microLED displays are transistors made of amorphous silicon, polycrystal, or single crystal Si, corresponding to  $\alpha$ -Si TFT, LTPS TFT, or CMOS [4].  $\alpha$ -Si TFT has been used in backplane technology for many years due to the advantage of low fabrication cost, simple and various manufacturing methods. However, in high luminance applications,  $\alpha$ -Si TFT panels have problems with threshold voltage shift and limit area of TFT owing to its low mobility [143]. LTPS TFT has ten times higher mobility than  $\alpha$ -Si TFT, resulting in a much faster switch rate and smaller chip size. It is the current primary technology used in AM organic LED (AMOLED).

CMOS provides more advantages than  $\alpha$ -Si TFT and LTPS TFT because monocrystalline silicon has a much better crystal quality and electrical properties, especially much higher mobility than amorphous Si and polycrystal Si. Moreover, single-crystal silicon circuits can be fabricated using well-developed Si IC equipment and processes in Si foundry. Si foundries can provide high-performance, high-reliable, and small-size CMOS at low cost. Furthermore, multiple functions ICs can be made in single crystalline silicon. Due to the small size of the CMOS driver, more circuitry can be integrated on the display surface for additional functions, or more room can be given to microLED for a higher EQE in high PPI applications. As a result, CMOS drivers can improve image quality, reduce device size, and lower the system's overall cost. However, due to the size limit of the Si wafer, a CMOS driver is only suitable to make small-screen displays, such as a projector and near-eye displays, except an additional mass transfer process is applied [144]. Moreover, the single-crystal silicon wafers are opaque. Therefore, CMOS microLED display cannot be used in an application requesting a transparent display and a high fill factor. Also, the cost of the CMOS is much higher than LTPS TFT.

**5.1.3. PMOS vs. NMOS.** Due to their superior performance, high mobility, good uniformity, and excellent reliability, CMOS based ICs will be the dominant technology for the control circuit in high-end small size displays, especially the near-eye applications, although its high cost. There are two types of

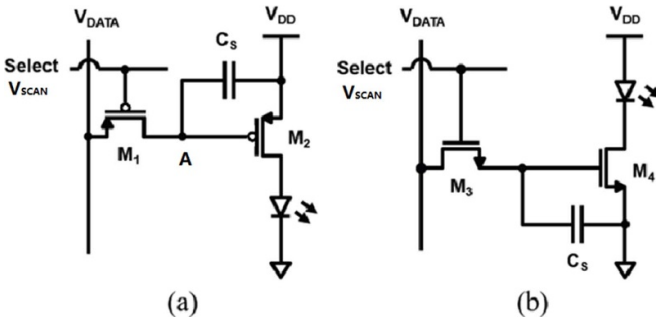


**Figure 43.** AM pixel driver in (a) PMOS and (b) NMOS configurations. © (2017) IEEE. Reprinted, with permission, from [145].

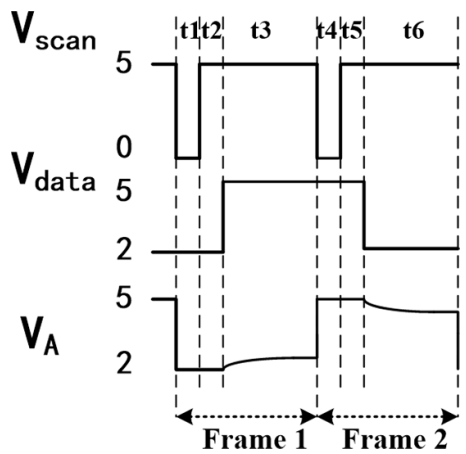


**Figure 44.** The timing diagram of two frames of the 2T1C AM pixel circuit using PMOS. © (2016) IEEE. Reprinted, with permission, from [151].

CMOS: n-type MOS (NMOS) and p-type MOS (PMOS). The commonly used AM driving circuit consists of the two transistors and one capacitor (2T1C), as shown in figures 43(a) and (b) for PMOS and NMOS configurations, respectively.

In conventional microLED arrays, the n-contacts in the GaN microLED array are usually connected to form a common cathode and individually anode. It is generally used because the p-layer is on the top of a standard GaN LED epitaxial structure, which is necessary due to the low conductivity of p-doped GaN and memory effect of the Mg dopant. However, a common cathode configuration may have a uniformity issue due to the different series resistance from the various distance between the n-GaN to each pixel. The individual anode and common cathode setup mainly support PMOS AM drive [145], while the individual cathode and common anode configuration support both PMOS and NMOS drive circuits. A common cathode is associated with PMOS benefits to achieving a high fill-factor design because of the smaller pixel. As a result, PMOS is widely used in the microLED display application currently.

NMOS is more suitable for high-speed applications, such as VLC, because of the NMOS AM circuit's advantages over PMOS. It is well known that the holes mobility in PMOS transistors is several times lower than electrons mobility in

NMOS transistors. Hence, the NMOS transistors are much faster. NMOS driving transistors (M<sub>2</sub> and M<sub>4</sub> in figure 43) have a lower gate capacitance at the same current, resulting in a higher operating speed of NMOS transistors. For the addressing transistors (M<sub>1</sub> and M<sub>3</sub> in figure 43), an NMOS transistor significantly lower resistance compared to a PMOS transistor of the same size. Such size limitation is often a vital design constraint in high PPI applications. An NMOS circuit can contain a larger pass transistor in the same area due to the smaller driving transistor [146]. Due to the smaller gate capacitance in the driving transistor and lower resistance in the pass transistor, the NMOS AM circuit has a lower RC time constant and faster operation. Liou *et al* compared AM driving circuits using PMOS and NMOS, and found that the resistance of the PMOS pass transistor is around three times higher [144]. Consequently, the variation in series resistance between microLED subpixels can be reduced by using NMOS drivers. Liou's simulation also shows that the NMOS circuit has a  $-3$  dB electrical bandwidth of 505 MHz compared to the bandwidth of 125 MHz in the PMOS circuit [144]. This advantage is significant for high-speed applications. Likewise, the common anode configuration is ideal in high-speed applications due to the ability to support NMOS driving.

**5.1.4. Voltage driving vs. current driving.** The AMLED using CMOS to control the luminance of microLEDs accurately can select a voltage across the microLED, i.e. voltage driving method, or a current flowing through the microLED, i.e. current driving method. The voltage driving approach has the advantages of simplicity of the driving circuit and low power consumption. However, it worsens the brightness uniformity due to significant forward voltages variation among microLEDs. Furthermore, the luminance/current exponentially changes with the applied voltage, leading to difficulty controlling the luminance. In contrast, the luminance of the microLED can be controlled linearly by the forward current in the current driving approach. Therefore, the current driving is widely used in microLED display applications. The microLED display with high but nonuniform luminance was achieved by a voltage driving approach [147]. The current driving approach is reported to improve luminance uniformity to 1.94% and 0.91% in a PMLED and AMLED displays, respectively [148, 149]. We believe current driving is a better choice in microLED display applications, and voltage driving is a better option in microLED VLC application.

**5.1.5. Mechanism of circuit design and operation.** It is using PMOS AM current control as an example to illustrate the design and operation mechanism of the driver for a single microLED. The two transistors in figure 43(a) are addressing transistor (M<sub>1</sub>) and driving transistor (M<sub>2</sub>), respectively. The LED pixel is working under the current control mode, so the  $I_{ds}$  of the driving transistor is decided by  $V_{gs}$  only when it works in an active region. The data signal is stored in the storage capacitor (C<sub>s</sub>), resulting in a continuous supplied current, keeping the pixel brightness throughout the period [150].

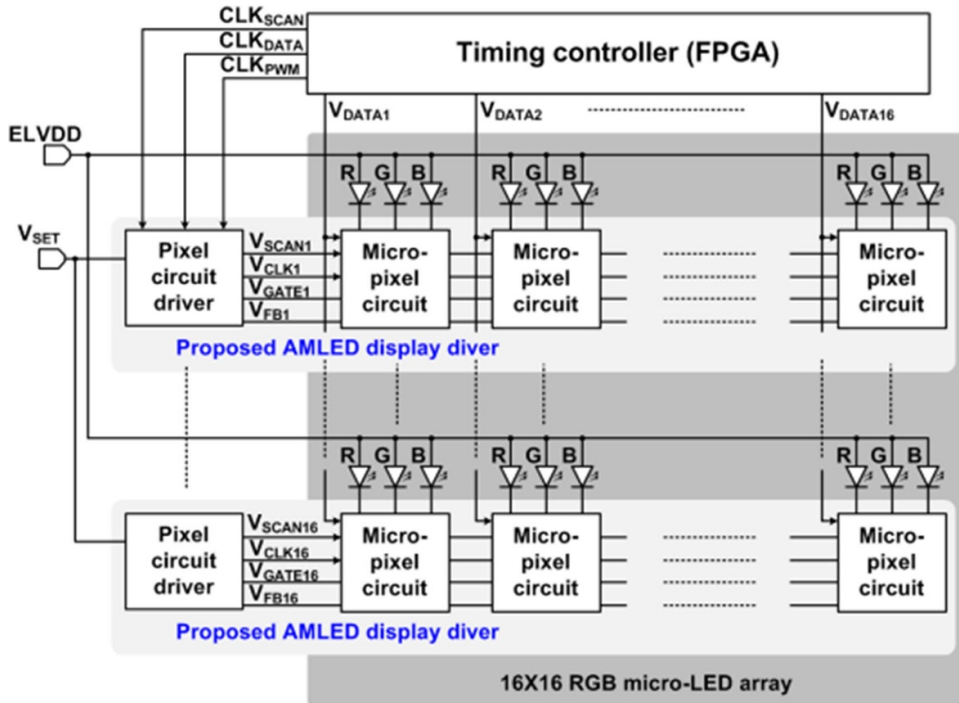


**Figure 45.** Block diagram of a typical AMLED display. © (2018) IEEE. Reprinted, with permission, from [149].

When  $V_{gs}$  is less than the threshold voltage ( $V_{th}$ ), that is  $-1\text{ V}$ , the transistor is switched ON, and the drain voltage of this transistor increases until it is equal to the source. The timing diagram of the 2T1C AM circuit operation is shown in figure 44 [151]. The LED pixel is ON in frame 1 and OFF in frame 2. Each frame has three parts.

The signal is written in period t1, in which the microLEDs is switched on. Period t2 is protection time, in which  $V_{scan}$  is staying at high voltage to prevent leakage of the signal stored in  $C_s$ . Period t3 is the holding time in which the pixel keeps on due to the continuous driving current from  $M2$  to the microLED. However, the leakage in  $M1$  causes a gradually reduced current through  $M2$ . Period t4 is the writing time in frame 2, in which the microLED is switched off. Likewise, t5 and t6 are the protection time and the holding time in frame 2 in which microLED stays in off [151].

The application-specific integrated circuits (ASICs) system of microLED display array is an architecture that uses serial input data and parallel output data. This circuit is a combined signal generating unit, counter, decoder, shift register, and latch register module [151]. Figure 45 is the block diagram of an AMLED display circuit, including a timing controller, microLED array, and AMLED drivers. A timing controller is a field-programmable gate array, generating clock signals ( $CLK_{SCAN}$ ,  $CLK_{DATA}$ , and  $CLK_{PWM}$ ) and digital data ( $V_{DATA}$ ), which represents the grayscale.  $CLK_{SCAN}$ ,  $CLK_{DATA}$ , and  $CLK_{PWM}$  are used to produce selection signals ( $V_{SCAN}$ ), data signal  $V_{DATA}$ , and PWM signal. The driver produces analog signals of  $V_{GATE}$  and  $V_{FB}$  to control the applied current through every subpixel and digital signals of  $V_{SCAN}$  and  $V_{CLK}$  to program  $V_{DATA}$  into the pixel circuit. Overall, the data processing unit reads both data and control signals from an

external microcontroller and then writes it into the RAM. The PWM generator reads the data from the RAM and produces PWM driving signals to the microLED array. The grey or color of the RGB pixels is controlled by PWM signals [152].

## 5.2. Backplane and panel fabrication

**5.2.1. Backplane preparation.** Currently, CMOS or LTPS are used as transistors for microLED display drivers. COMS backplane is fabricated in semiconductor foundry by Bipolar-CMOS-DMOS technology. The standard CMOS processes of  $0.18\text{--}0.35\text{ }\mu\text{m}$  are selected to make CMOS for microLED array drivers based on the performance and size requirements. High-voltage transistors of  $10\text{ V}\text{--}40\text{ V}$  are available in semiconductor foundries.  $10\text{ V}/12\text{ V}$  high voltage transistors and  $5\text{ V}/6\text{ V}$  middle voltage transistors are usually used in microLED display applications.

A typical example to make an LTPS backplane is described below. LTPS TFT backplane is made over glass substrates with a coplanar or staggered structure. A  $400\text{ nm}$  thick  $\text{SiO}_2$  layer is deposited on a glass substrate by sputtering, and then a  $90\text{ nm}$  thick LTPS is formed as an active layer by laser annealing [153]. A  $100\text{ nm}$  thick  $\text{SiO}_2$  is deposited as a gate insulator by PECVD, and then a  $200\text{ nm}$  thick Mo layer is deposited as gate and source and drain electrodes. Finally, A  $650\text{ nm}$  thick  $\text{SiO}_2/\text{SiN}_x$  layer is deposited as a passivation layer by PECVD, and then a  $400\text{ nm}$  Mo–Au layer is used as metal to bond microLEDs on the TFT backplane [154].

Figure 46 shows a schematic layout of the common anode configuration to emphasize the electrode [122]. The conductive path is formed by a Ti/Au metal bilayer instead of n-GaN in traditional common cathode configuration. Although

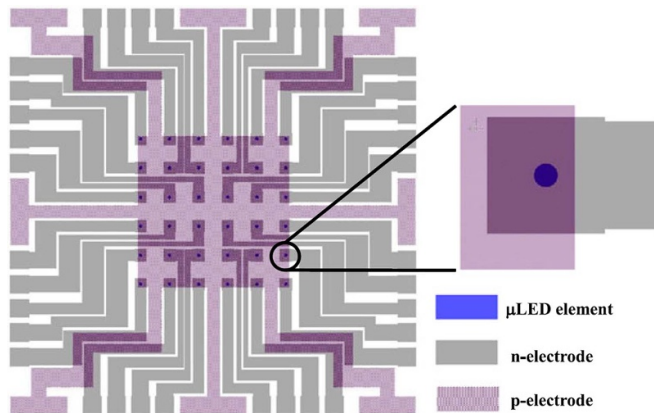


**Figure 46.** Shows a schematic layout of a  $6 \times 6$  common anode microLED array. Reproduced from [122]. CC BY 4.0.

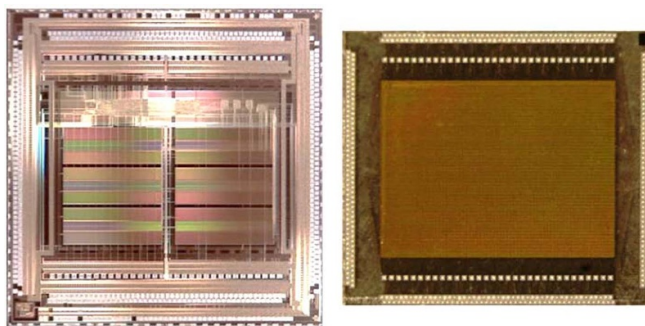


**Figure 47.** ASIC driver and microLED array before bonding. © (2014) IEEE. Reprinted, with permission, from [152].

there are still different distances between the electrode and the target microLED element, the resulting series resistance difference is minimal because the sheet resistivity of the metal layer is significantly lower. Figure 47 shows the images of the ASIC display driver and microLED array before bonding. MicroLED array is bonded on LTPS/CMOS TFT backplane to make a panel [152].

**5.2.2. Bonding processing to build a panel.** Below is a typical process to bond the microLED onto LTPS or CMOS substrates [82, 152, 155, 156]. A submicron-thick dielectric layer is deposited by PECVD first. The dielectric protective layer could be  $\text{SiN}_x$  or  $\text{SiO}_2$  materials. The opening pattern is defined by the photolithography process. The dielectric layer is then removed to reveal the P-type metal contact electrode by ICP or RIE etching. Bonding metal is used for mechanically and electrically connection between the drivers and microLED array. To get a high-quality bonding layer, Au-based metallic, such as Au/In [157] and Au/Sn [158] are used as the bonding metal materials, but the high cost of the Au raises the cost of microLED displays. Hence Au-free metal bonding is highly desirable. Lay *et al* demonstrated an Au-free bonding material, Cu/Sn-based bonding metal, in microLED [159]. Indium is another Au-free option. As shown in figure 48(a), indium plates are deposited on electrode pads of the microLED array by evaporation. The indium ball is formed by reflowing,

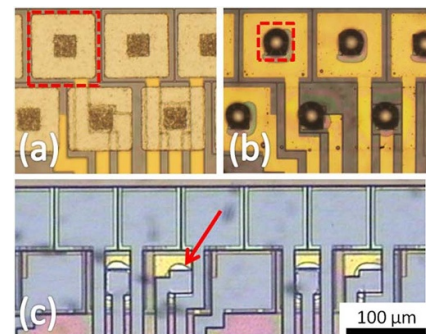


**Figure 48.** Microscopic images of microLED arrays with (a) indium plates; (b) indium balls formed by reflowing; (c) after bonding on backplane. © (2014) IEEE. Reprinted, with permission, from [152].

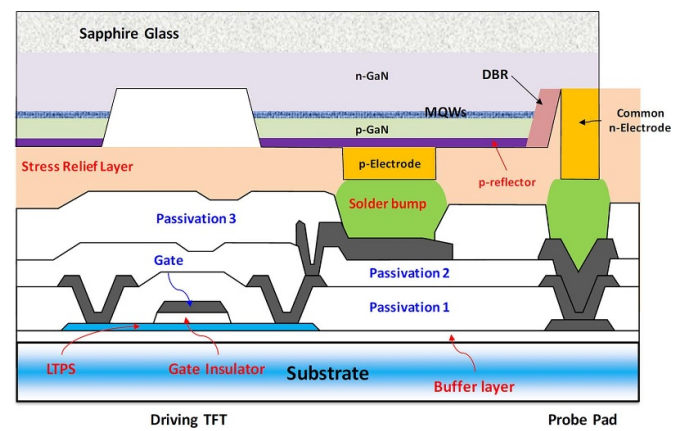


**Figure 49.** Schematic structure of AMLEDs using a bump bonding method. [154] John Wiley & Sons. Copyright © 2018 WILEY-VCH Verlag GmbH & Co. KGaA, Weinheim.

shown in figure 48(b). Finally, the microLED array is bonded with drivers on the backplane by a die bonder, as shown in figure 48(c). The alignment accuracy of the flip-chip bonder is  $1 \mu\text{m}$ . After bonding, it is filled with underfill to fix the microLEDs array, passivate the devices, and planarize the backplane. Benzocyclobutene is usually used as the underfill material. It is coated by a spin coating process and etched back to reveal the devices [152].

Figure 49 shows the cross-sectional view of a typical flip-chip microLED bonded on the LTPS TFT. The p-electrode on the p-GaN of the microLED connects to the LTPS TFT via the solder, and the nGaN layer is connected to the common n-electrode [154]. The stress relief layer and several passivation layers are used between the microLED and TFT driver.

### 5.3. Technologies to improve panel performance

The microlens is proposed to improve the extraction efficiency and control the emission direction of the microLED as early as 2003 [160]. Choi *et al* fabricated microlens on the sapphire surface at the position aligning to the microLED, and improved efficiency by around 15%, as shown in figure 50. The microlens is made using a thermal resist reflow technique.

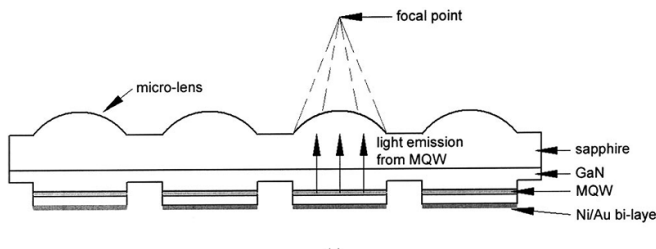


**Figure 50.** Schematic of the microlens on the sapphire aligning to the microLED. Reprinted from [160], with the permission of AIP Publishing.

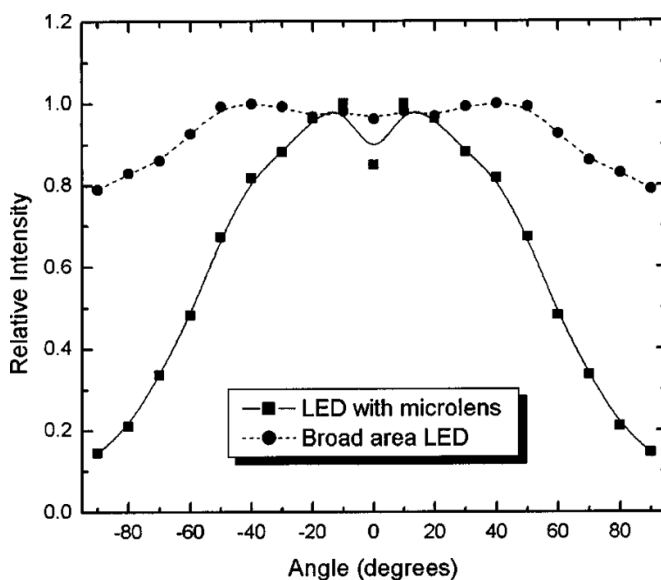


**Figure 51.** Radiation pattern comparison of the microLED with a microlens and the broad-area LED without lens. Reprinted from [160], with the permission of AIP Publishing.

The photoresist is coated and patterned into a disk shape first. Then, the pattern is transferred to the sapphire by dry etching.

Microlens can change the radiation characteristics of the microLEDs. A comparison of the radiation

patterns from a LED with and without microlens is shown in figure 51 [160]. The microlens array collects light emitted from the MQWs into a direction normal to MQWs, resulting in more than 80% of the light-emitting within an angle  $<40^\circ$ . The light thus can be engineered by optics if necessary. Microlenses with different sizes, materials, and various locations are proposed to improve efficiency and collimate the light. Demory *et al* fabricated a SiN nano lens array coupled to a microLED color array. They demonstrated a 95% emission collimated within a 0.5 aperture and a 350% efficiency increase, compared to the LED without a lens [161].

A significant blueshift of the emission wavelength of the MQWs as the current increase is a challenging problem to be solved in polar III-nitride microLED. PWM is used to control the wavelength drift caused by current density change. On another side, Gong *et al* took advantage of such color shift and

demonstrated a programmable color-tunable microLED display with relevant custom CMOS technology, based on one InGaN structure [162].

Luminance and color nonuniformity are severe issues in microLED display panels because the epitaxial wafer uniformity is not as good as OLED and LCD. Various techniques have been proposed to mitigate brightness nonuniformity in the AMLED display system. One solution is using external compensation circuitry [163, 164]. Qiu *et al* proposed a novel time-interleaving analog adder with the nonlinear error reduced to 0.0735% [165]. Ahn *et al* also used compensation drivers for resistance mismatch and achieved an average current deviation of 0.91% [149], which was much smaller than the deviation of 10.0% [147] and 1.94% [148] obtained in previous reports. Additionally, this compensation driver [166] reduced the current rising time from previously reported 1.1  $\mu$ s to 480 ns [149].

## 6. Outlook remarks

MicroLED has many advantages compared with current LCD and OLED displays, leading to a wide range of applications and huge markets. At the same time, the tiny chip size and high requirements for display applications cause many problems and strict specifications in each manufacturing step. From epitaxial wafer growth to panel manufacturing, the long supply chain also causes problems in the entire system design and complex processes. Fortunately, due to its broad and novel applications, microLED has attracted extensive attention from many companies and research teams. Therefore, fruitful results have been continuously achieved. For example, the recent developments from the UCSB and other teams shed light on solving the major challenge of lower EQE of smaller microLEDs for the first time. We believe that problem solving will be expedited as more groups join this research. MicroLED has a bright future. It will become the next-generation technology for traditional displays such as AR, VR, MR, smartphones, automobiles, laptop screens, HDTVs, as well as new types of displays such as flexible displays, wearable devices, transparent displays, and field displays. It also creates new applications, including VLC, Lithography, medical equipment, etc due to its unique characteristics.

## ORCID iDs

Zhen Chen <https://orcid.org/0000-0002-3880-6232>

Shuke Yan <https://orcid.org/0000-0002-0171-7906>

Cameron Danesh <https://orcid.org/0000-0002-3518-989X>

## References

- [1] Tan G, Huang Y, Li M-C, Lee S-L and Wu S-T 2018 High dynamic range liquid crystal displays with a mini-LED backlight *Opt. Express* **26** 16572
- [2] Jiang H X, Jin S X, Li J, Shakya J and Lin J Y 2001 III-nitride blue microdisplays *Appl. Phys. Lett.* **78** 1303–5
- [3] Zhang H X, Massoubre D, McKendry J, Gong Z, Guilhabert B, Griffin C, Gu E, Jessop P E, Girkin J M and

- Dawson M D 2008 Individually-addressable flip-chip AlInGaN micropixelated light emitting diode arrays with high continuous and nanosecond output power *Opt. Express* **16** 9918
- [4] Liu Z J, Wong K M, Keung C W, Tang C W and Lau K M 2009 Monolithic LED microdisplay on active matrix substrate using flip-chip technology *IEEE J. Sel. Top. Quantum Electron.* **15** 1298–302
- [5] Virey E 2018 Are microLEDs really the next display revolution? *Inf. Disp.* **34** 22–27
- [6] Moore S K 2019 Microled displays expected in 2020: the last remaining hurdle is mastering mass production—[News] *IEEE Spectr.* **56** 8–9
- [7] Kajiyama Y, Kajiyama K and Aziz H 2015 Maskless RGB color patterning of vacuum-deposited small molecule OLED displays by diffusion of luminescent dopant molecules *Opt. Express* **23** 16650
- [8] Lee -C-C, Shih Y-S, Wu C-S, Tsai C-H, Yeh S-T, Peng Y-H and Chen K-J 2012 Development of robust flexible OLED encapsulations using simulated estimations and experimental validations *J. Phys. D: Appl. Phys.* **45** 275102
- [9] Park M-H, Kim J-Y, Han T-H, Kim T-S, Kim H and Lee T-W 2015 Flexible encapsulation: flexible lamination encapsulation (Adv. Mater. 29/2015) *Adv. Mater.* **27** 4387–4387
- [10] Spindler J P, Hatwar T K, Miller M E, Arnold A D, Murdoch M J, Kane P J, Ludwicki J E, Alessi P J and van Slyke S A 2006 System considerations for RGBW OLED displays *J. Soc. Inf. Disp.* **14** 37–48
- [11] Tian P, Althumali A, Gu E, Watson I M, Dawson M D and Liu R 2016 Aging characteristics of blue InGaN micro-light emitting diodes at an extremely high current density of 3.5 kA cm<sup>-2</sup> *Semicond. Sci. Technol.* **31** 045005
- [12] Haas G 2018 40-2: invited paper: microdisplays for augmented and virtual reality *SID Symposium Digest of Technical Papers* pp 506–9
- [13] Liu Z, Chong W C, Wong K M and Lau K M 2015 GaN-based LED micro-displays for wearable applications *Microelectron. Eng.* **148** 98–103
- [14] Haas G 2019 52-1: Invited Paper: Microdisplays for Wearable Augmented Reality — OLED vs LED Based Systems *SID Symposium Digest of Technical Papers* pp 713–6
- [15] Park S-I *et al* 2009 Printed assemblies of inorganic light-emitting diodes for deformable and semitransparent displays *Science* **325** 977–81
- [16] Kim T I *et al* 2013 Injectable, cellular-scale optoelectronics with applications for wireless optogenetics *Science* **340** 211–6
- [17] Klein E, Gossler C, Paul O and Ruther P 2018 High-density  $\mu$ LED-based optical cochlear implant with improved thermomechanical behavior *Front. Neurosci.* **12** 659
- [18] Poher V *et al* 2008 Micro-LED arrays: a tool for two-dimensional neuron stimulation *J. Phys. D: Appl. Phys.* **41** 094014
- [19] Mickle A D *et al* 2019 A wireless closed-loop system for optogenetic peripheral neuromodulation *Nature* **565** 361–5
- [20] Alpaslan Z Y and El-Ghoroury H S 2015 Small form factor full parallax tiled light field display *Stereoscopic Displays and Applications XXVI* 9391 (SPIE) pp 93910E
- [21] El-Ghoroury H S and Chuang C L 2015 26.1:Invited Paper: Quantum Photonic Imager (QPI): A Novel Display Technology that Enables more than 3D Applications *SID Symposium Digest of Technical Papers* pp 371–4
- [22] McKendry J J D, Green R P, Kelly A E, Gong Z, Guilhabert B, Massoubre D, Gu E and Dawson M D 2010 High-speed visible light communications using individual pixels in a micro light-emitting diode array *IEEE Photonics Technol. Lett.* **22** 1346–8
- [23] Khalid A M, Cossu G, Corsini R, Choudhury P and Ciaramella E 2012 1-Gb/s transmission over a phosphorescent white LED by using rate-adaptive discrete multitone modulation *IEEE Photonics J.* **4** 1465–73
- [24] Islim M S *et al* 2017 Towards 10 Gb/s orthogonal frequency division multiplexing-based visible light communication using a GaN violet micro-LED *Photonics Res.* **5** A35
- [25] Lin C-H, Lee C-F, Lin C-C, Chu C-H, Sher C-W, Liu Z-J and Kuo H-C 2018 25.1: Invited Paper: Quantum dots based full-color display on micro-light-emitting-diode technology *SID Symposium Digest of Technical Papers* pp 267–70
- [26] Lin J Y and Jiang H X 2020 Development of microLED *Appl. Phys. Lett.* **116** 100502
- [27] Lee V W, Twu N and Kymmissis I 2016 Micro-LED technologies and applications *Inf. Disp.* **32** 16–23
- [28] Virey E H, Baron N and Bouhamri Z 2019 Overlooked Challenges for microLED Displays *SID Symposium Digest of Technical Papers* **50** pp 129–32
- [29] Barrigón E, Heurlin M, Bi Z, Monemar B and Samuelson L 2019 Synthesis and applications of III–V nanowires *Chem. Rev.* **119** 9170–220
- [30] Narukawa Y, Ichikawa M, Sanga D, Sano M and Mukai T 2010 White light emitting diodes with super-high luminous efficacy *J. Phys. D: Appl. Sci.* **43** 354002
- [31] Krames M R *et al* 1999 High-power truncated-inverted-pyramid (Al<sub>x</sub>Ga<sub>1-x</sub>)<sub>0.5</sub>In<sub>0.5</sub>P/GaP light-emitting diodes exhibiting >50% external quantum efficiency *Appl. Phys. Lett.* **75** 2365–7
- [32] Bulashevich K A and Karpov S Y 2016 Impact of surface recombination on efficiency of III-nitride light-emitting diodes *Phys. Status Solidi RRL* **10** 480–4
- [33] Aleksiejūnas R, Gelžintė K, Nargelės S, Jarašiūnas K, Vengris M, Armour E A, Byrnes D P, Arif R A, Lee S M and Papasouliotis G D 2014 Diffusion-driven and excitation-dependent recombination rate in blue InGaN/GaN quantum well structures *Appl. Phys. Lett.* **104** 022114
- [34] Malinauskas T *et al* 2012 Impact of carrier localization, recombination, and diffusivity on excited state dynamics in InGaN/GaN quantum wells *SPIE* p 82621S
- [35] Prasad M, Martinez O E, Menoni C S, Rocca J J, Chilla J L A, Hafich M J and Robinson G Y 1994 Transient grating measurements of ambipolar diffusion and carrier recombination in InGaP/lnAlP multiple quantum wells and InGaP bulk *J. Electron. Mater.* **23** 359–62
- [36] Thiagarajan P, Schmerge J F, Menoni C S, Marconi M, Martinez O E, Rocca J J, Hafich M J, Lee H Y and Robinson G Y 1991 Picosecond absorption dynamics of photoexcited InGaP epitaxial films *Appl. Phys. Lett.* **59** 90–92
- [37] Kitagawa H, Fujita M, Suto T, Asano T and Noda S 2011 Green GaInN photonic-crystal light-emitting diodes with small surface recombination effect *Appl. Phys. Lett.* **98** 181104
- [38] Onuma T, Sakai N, Igaki T, Yamaguchi T, Yamaguchi A A and Honda T 2012 Comparative study of surface recombination in hexagonal GaN and ZnO surfaces *J. Appl. Phys.* **112** 063509
- [39] Smith J M, Ley R, Wong M S, Baek Y H, Kang J H, Kim C H, Gordon M J, Nakamura S, Speck J S and DenBaars S P 2020 Comparison of size-dependent characteristics of blue and green InGaN microLEDs down to 1  $\mu$ m in diameter *Appl. Phys. Lett.* **116** 071102
- [40] Lee H K, Lee D H, Song Y M, Lee Y T and Yu J S 2011 Thermal measurements and analysis of AlGaInP/GaInP MQW red LEDs with different chip sizes and substrate thicknesses *Solid State Electron.* **56** 79–84

- [41] Lee C-T, Cheng C-J, Lee H-Y, Chu Y-C, Fang Y-H, Chao C-H and Wu M-H 2015 Color conversion of GaN-based micro light-emitting diodes using quantum dots *IEEE Photonics Technol. Lett.* **27** 2296–9
- [42] Boyd A R, Beckers A, Eickelkamp M, Alam A and Heukens M 2019 Enabling MOCVD Technology for Micro LED High Volume Manufacturing *SID Symposium Digest of Technical Papers* pp 342–5
- [43] Beckers A, Fahle D, Mauder C, Kruecken T, Boyd A R and Heukens M 2018 Invited Paper: Enabling the Next Era of Display Technologies by Micro LED MOCVD Processing *SID Symposium Digest of Technical Papers* pp 601–3
- [44] Berglund C N 1996 A unified yield model incorporating both defect and parametric effects *IEEE Trans. Semicond. Manuf.* **9** 447–54
- [45] Murphy B T 1964 Cost-size optima of monolithic integrated circuits *Proc. IEEE* **52** 1537–45
- [46] Paranjape A, Montgomery J, Lee S M and Morath C 2018 45–2: Invited Paper: Micro-LED Displays: Key Manufacturing Challenges and Solutions *SID Symposium Digest of Technical Papers* pp 597–600
- [47] Chen H, He J and Wu S-T 2017 Recent advances on quantum-dot-enhanced liquid-crystal displays *IEEE J. Sel. Top. Quantum Electron.* **23** 1–11
- [48] Yamada M, Mitani T, Narukawa Y, Shioji S, Niki I, Sonobe S, Deguchi K, Sano M and Mukai T 2002 InGaN-based near-ultraviolet and blue-light-emitting diodes with high external quantum efficiency using a patterned sapphire substrate and a mesh electrode *Japan. J. Appl. Phys.* **41** L1431–3
- [49] Wang T-Y, Tasi C-T, Lin K-Y, Ou S-L, Horng R-H and Wu D-S 2018 Surface evolution and effect of V/III ratio modulation on etch-pit-density improvement of thin AlN templates on nano-patterned sapphire substrates by metalorganic chemical vapor deposition *Appl. Surf. Sci.* **455** 1123–30
- [50] Lee F-W, Ke W-C, Cheng C-H, Liao B-W and Chen W-K 2016 Influence of different aspect ratios on the structural and electrical properties of GaN thin films grown on nanoscale-patterned sapphire substrates *Appl. Surf. Sci.* **375** 223–9
- [51] Park S-H and Chuang S-L 1999 Crystal-orientation effects on the piezoelectric field and electronic properties of strained wurtzite semiconductors *Phys. Rev. B* **59** 4725–37
- [52] Craven M D, Lim S H, Wu F, Speck J S and DenBaars S P 2002 Structural characterization of nonpolar (1120) a-plane GaN thin films grown on (1102) r-plane sapphire *Appl. Phys. Lett.* **81** 469–71
- [53] Chen Z, Lu D-C, Wang X, Liu X, Yuan H, Han P, Wang D, Wang Z and Li G 2002 The mechanism of blueshift in excitation-intensity-dependent photoluminescence spectrum of nitride multiple quantum wells *J. Lumin.* **99** 35–38
- [54] Marion F, Bisotto S, Berger F, Gueugnot A, Mathieu L, Henry D, Templier F and Catelain T 2016 A room temperature flip-chip technology for high pixel count micro-displays and imaging arrays *2016 IEEE 66th Electronic Components and Technology Conf. (ECTC)* pp 929–35
- [55] Zhang S *et al* 2020 Efficient emission of InGaN-based light-emitting diodes: toward orange and red *Photonics Res.* **8** 1671–5
- [56] Dayeh S, Jagadish C and Fontcuberta Morral A 2016 Semiconductors and semimetals *Semiconductor Nanowires II: Properties and Applications* vol 94 (Cambridge, MA: Elsevier)
- [57] Yamamoto A, Sugita K and Hashimoto A 2009 Elucidation of factors obstructing quality improvement of MOVPE-grown InN *J. Cryst. Growth* **311** 4636–40
- [58] Mesrine M, Grandjean N and Massies J 1998 Efficiency of NH<sub>3</sub> as nitrogen source for GaN molecular beam epitaxy *Appl. Phys. Lett.* **72** 350–2
- [59] Tauzin A *et al* 2005 Transfers of 2-inch GaN films onto sapphire substrates using Smart Cut™ technology *Electron. Lett.* **41** 668
- [60] Even A, Laval G, Ledoux O, Ferret P, Sotta D, Guiot E, Levy F, Robin I-C and Dussaigne A 2017 Enhanced In incorporation in full InGaN heterostructure grown on relaxed InGaN pseudo-substrate *Appl. Phys. Lett.* **110** 262103
- [61] Ozaki T, Funato M and Kawakami Y 2019 Red-emitting In<sub>x</sub> Ga 1-x N/In<sub>y</sub> Ga 1-y N quantum wells grown on lattice-matched In<sub>y</sub> Ga 1-y N/ScAlMgO 4 (0001) templates *Appl. Phys. Express* **12** 011007
- [62] Yoshikawa A, Che S B, Yamaguchi W, Saito H, Wang X Q, Ishitani Y and Hwang E S 2007 Proposal and achievement of novel structure InGaN multiple quantum wells consisting of 1 ML and fractional monolayer InN wells inserted in GaN matrix *Appl. Phys. Lett.* **90** 073101
- [63] Gorczyca I, Suski T, Strak P, Staszczak G and Christensen N E 2017 Band gap engineering of In(Ga)N/GaN short period superlattices *Sci. Rep.* **7** 16055
- [64] Yoshikawa A, Hashimoto N, Kikukawa N, Che S B and Ishitani Y 2005 Growth of InN quantum dots on N-polarity GaN by molecular-beam epitaxy *Appl. Phys. Lett.* **86** 153115
- [65] Doppalapudi D, Basu S N, Ludwig K F and Moustakas T D 1998 Phase separation and ordering in InGaN alloys grown by molecular beam epitaxy *J. Appl. Phys.* **84** 1389–95
- [66] Zhu W, Mitchell B, Timmerman D, Koizumi A, Gregorkiewicz T and Fujiwara Y 2017 High-power Eu-doped GaN red LED based on a multilayer structure grown at lower temperatures by organometallic vapor phase epitaxy *MRS Adv.* **2** 159–64
- [67] Mitchell B, Dierolf V, Gregorkiewicz T and Fujiwara Y 2018 Perspective: toward efficient GaN-based red light emitting diodes using europium doping *J. Appl. Phys.* **123** 160901
- [68] Shioda T, Yoshida H, Tachibana K, Sugiyama N and Nunoue S 2012 Enhanced light output power of green LEDs employing AlGaN interlayer in InGaN/GaN MQW structure on sapphire (0001) substrate *Phys. Status Solidi a* **209** 473–6
- [69] Saito S, Hashimoto R, Hwang J and Nunoue S 2013 InGaN light-emitting diodes on c-face sapphire substrates in green gap spectral range *Appl. Phys. Express* **6** 111004
- [70] Hwang J, Hashimoto R, Saito S and Nunoue S 2014 Development of InGaN-based red LED grown on (0001) polar surface *Appl. Phys. Express* **7** 071003
- [71] Calleja E, Sánchez-García M A, Sánchez F J, Calle F, Naranjo F B, Muñoz E, Jahn U and Ploog K 2000 Luminescence properties and defects in GaN nanocolumns grown by molecular beam epitaxy *Phys. Rev. B* **62** 16826–34
- [72] Sekiguchi H, Nakazato T, Kikuchi A and Kishino K 2007 Structural and optical properties of GaN nanocolumns grown on (0001) sapphire substrates by RF-plasma-assisted molecular-beam epitaxy *J. Cryst. Growth* **300** 259–62
- [73] Li S and Waag A 2012 GaN based nanorods for solid state lighting *J. Appl. Phys.* **111** 071101
- [74] Sekiguchi H, Kishino K and Kikuchi A 2010 Emission color control from blue to red with nanocolumn diameter of InGaN/GaN nanocolumn arrays grown on same substrate *Appl. Phys. Lett.* **96** 231104
- [75] Gilet P and Robin I-C 2018 52-1: *Invited paper:* nanostructures on silicon to solve the active display paradigms *SID Symposium Digest of Technical Papers* pp 684–7

- [76] Yang S-M, Wang P-H, Chao C-H, Chu C-W, Chen Y-S, Chang F-P, Fang Y-H, Lin -C-C and Wu C-I 2019 P-127: The Substrate Thickness Dependence on Micro LED Chip Arrays *SID Symposium Digest of Technical Papers* pp 1724–7
- [77] Li K H, Cheung Y F, Cheung W S and Choi H W 2015 Confocal microscopic analysis of optical crosstalk in GaN micro-pixel light-emitting diodes *Appl. Phys. Lett.* **107** 171103
- [78] Li K H, Cheung Y F, Tang C W, Zhao C, Lau K M and Choi H W 2016 Optical crosstalk analysis of micro-pixelated GaN-based light-emitting diodes on sapphire and Si substrates *Phys. Status Solidi a* **213** 1193–8
- [79] Horng R H, Chien H Y, Tarnair F G and Wuu D S 2018 Fabrication and study on red light micro-LED displays *IEEE J. Electron Devices Soc.* **6** 1064–9
- [80] Chen C J, Chen H C, Liao J H, Yu C J and Wu M C 2019 Fabrication and characterization of active-matrix 960 × 540 blue GaN-based micro-LED display *IEEE J. Quantum Electron.* **55** 3300106
- [81] Gou F, Hsiang E-L, Tan G, Lan Y F, Tsai C Y and Wu S T 2019 High performance color-converted micro-LED displays *J. Soc. Inf. Disp.* **27** 199–206
- [82] Day J, Li J, Lie D Y C, Bradford C, Lin J Y and Jiang H X 2011 III-Nitride full-scale high-resolution microdisplays *Appl. Phys. Lett.* **99** 031116
- [83] Bai X, Yang H, Zhao B, Zhang X, Li X, Xu B, Wei F, Liu Z, Wang K and Sun X W 2019 4-4: Flexible Quantum Dot Color Converter Film for Micro-LED Applications *SID Symposium Digest of Technical Papers* pp 30–3
- [84] Kim H M, Ryu M, Cha J H J, Kim H S, Jeong T and Jang J 2019 Ten micrometer pixel, quantum dots color conversion layer for high resolution and full color active matrix micro-LED display *J. Soc. Inf. Disp.* **27** 347–53
- [85] Han H-V *et al* 2015 Resonant-enhanced full-color emission of quantum-dot-based micro LED display technology *Opt. Express* **23** 32504
- [86] Lee E *et al* 2018 41-5: *Invited paper:* quantum dot conversion layers through inkjet printing pp 525–7
- [87] Huang Chen S-W *et al* 2019 Full-color monolithic hybrid quantum dot nanoring micro light-emitting diodes with improved efficiency using atomic layer deposition and nonradiative resonant energy transfer *Photonics Res.* **7** 416
- [88] Dai L, Zhang B, Lin J Y and Jiang H X 2001 Comparison of optical transitions in InGaN quantum well structures and microdisks *J. Appl. Phys.* **89** 4951–4
- [89] Choi H W, Jeon C W, Dawson M D, Edwards P R, Martin R W and Tripathy S 2003 Mechanism of enhanced light output efficiency in InGaN-based microlight emitting diodes *J. Appl. Phys.* **93** 5978–82
- [90] Tian P, McKendry J J D, Gong Z, Guilhabert B, Watson I M, Gu E, Chen Z, Zhang G and Dawson M D 2012 Size-dependent efficiency and efficiency droop of blue InGaN micro-light emitting diodes *Appl. Phys. Lett.* **101** 231110
- [91] Olivier F, Tirano S, Dupré L, Aventurier B, Largeron C and Templier F 2017 Influence of size-reduction on the performances of GaN-based micro-LEDs for display application *J. Lumin.* **191** 112–6
- [92] Konoplev S S, Bulashevich K A and Karpov S Y 2018 From large-size to micro-LEDs: scaling trends revealed by modeling *Phys. Status Solidi a* **215** 1700508
- [93] Olivier F, Daami A, Dupré L, Henry F, Aventurier B and Templier F 2017 25-4: Investigation and Improvement of 10µm Pixel-pitch GaN-based Micro-LED Arrays with Very High Brightness *SID Symposium Digest of Technical Papers* pp 353–6
- [94] Karpov S 2015 ABC-model for interpretation of internal quantum efficiency and its droop in III-nitride LEDs: a review *Opt. Quantum Electron.* **47** 1293–303
- [95] Piprek J 2010 Efficiency droop in nitride-based light-emitting diodes *Phys. Status Solidi a* **207** 2217–25
- [96] Olivier F, Daami A, Licitra C and Templier F 2017 Shockley-Read-Hall and Auger non-radiative recombination in GaN based LEDs: a size effect study *Appl. Phys. Lett.* **111** 022104
- [97] Ley R T, Smith J M, Wong M S, Margalith T, Nakamura S, DenBaars S P and Gordon M J 2020 Revealing the importance of light extraction efficiency in InGaN/GaN microLEDs via chemical treatment and dielectric passivation *Appl. Phys. Lett.* **116** 251104
- [98] Choi H W, Jeon C W, Dawson M D, Edwards P R and Martin R W 2003 Fabrication and performance of parallel-addressed InGaN micro-LED arrays *IEEE Photonics Technol. Lett.* **15** 510–2
- [99] Gou F, Hsiang E-L, Tan G, Chou P-T, Li Y-L, Lan Y-F and Wu S-T 2019 Angular color shift of micro-LED displays *Opt. Express* **27** A746
- [100] Lobo Ploch N *et al* 2013 Effective thermal management in ultraviolet light-emitting diodes with micro-LED arrays *IEEE Trans. Electron Devices* **60** 782–6
- [101] Gong Z, Jin S, Chen Y, McKendry J, Massoubre D, Watson I M, Gu E and Dawson M D 2010 Size-dependent light output, spectral shift, and self-heating of 400 nm InGaN light-emitting diodes *J. Appl. Phys.* **107** 013103
- [102] McKendry J J D, Massoubre D, Zhang S, Rae B R, Green R P, Gu E, Henderson R K, Kelly A E and Dawson M D 2012 Visible-light communications using a CMOS-controlled micro-light-emitting-diode array *J. Lightwave Technol.* **30** 61–67
- [103] Li X, Bamiedakis N, Wei J, McKendry J J D, Xie E, Ferreira R, Gu E, Dawson M D, Penty R V and White I H 2015 µLED-based single-wavelength bi-directional POF link with 10 Gb/s aggregate data rate *J. Lightwave Technol.* **33** 3571–6
- [104] Moe C G *et al* 2010 Current-induced degradation of high performance deep ultraviolet light emitting diodes *Appl. Phys. Lett.* **96** 213512
- [105] Liu L, Ling M, Yang J, Xiong W, Jia W and Wang G 2012 Efficiency degradation behaviors of current/thermal co-stressed GaN-based blue light emitting diodes with vertical-structure *J. Appl. Phys.* **111** 093110
- [106] Chang M-H, Das D, Varde P V and Pecht M 2012 Light emitting diodes reliability review *Microelectron. Reliab.* **52** 762–82
- [107] Cao X A, Sandvik P M, LeBoeuf S F and Arthur S D 2003 Defect generation in InGaN/GaN light-emitting diodes under forward and reverse electrical stresses *Microelectron. Reliab.* **43** 1987–91
- [108] Polyakov A Y *et al* 2002 Enhanced tunneling in GaN/InGaN multi-quantum-well heterojunction diodes after short-term injection annealing *J. Appl. Phys.* **91** 5203–7
- [109] Yang Y and Cao X A 2009 Removing plasma-induced sidewall damage in GaN-based light-emitting diodes by annealing and wet chemical treatments *J. Vac. Sci. Technol. B* **27** 2337–41
- [110] Wong M S, Hwang D, Alhassan A I, Lee C, Ley R, Nakamura S and DenBaars S P 2018 High efficiency of III-nitride micro-light-emitting diodes by sidewall passivation using atomic layer deposition *Opt. Express* **26** 21324
- [111] Yang C-M, Kim D-S, Park Y S, Lee J-H, Lee Y S and Lee J-H 2012 Enhancement in light extraction efficiency of GaN-based light-emitting diodes using double dielectric surface passivation *Opt. Photonics J.* **02** 185–92

- [112] Zhu J, Takahashi T, Ohori D, Endo K, Samukawa S, Shimizu M and Wang X-L 2019 Near-complete elimination of size-dependent efficiency decrease in GaN micro-light-emitting diodes *Phys. Status Solidi a* **216** 1900380
- [113] Samukawa S 2015 A neutral beam process for controlling surface defect generation and chemical reactions at the atomic layer *ECS J. Solid State Sci. Technol.* **4** N5089–94
- [114] Higo A *et al* 2015 Light-emitting devices based on top-down fabricated GaAs quantum nanodisks *Sci. Rep.* **5** 9371
- [115] Fletcher R M, Kuo C P, Osentowski T D, Huang K H, Crawford M G and Robbins V M 1991 The growth and properties of high performance AlGaNp emitters using a lattice mismatched GaP window layer *J. Electron. Mater.* **20** 1125–30
- [116] Ettenberg M H, Lange M J, Sugg A R, Cohen M J and Olsen G H 1999 Zinc diffusion in InAsP/InGaAs heterostructures *J. Electron. Mater.* **28** 1433–9
- [117] Vanhollebeke K, D'Hondt M, Moerman I, van Daele P and Demeester P 2001 MOVPE based Zn diffusion into InP and InAsP/InP heterostructures *J. Cryst. Growth* **233** 132–40
- [118] Lee H J, Kim S U, So S J, Cho Y D, Kim Y J, Ahn S C and Lee C H 2013 Reduction of surface defects on the GaP window layer of 630 nm AlGaInP LED using post-Zn diffusion process *Curr. Appl. Phys.* **13** 1032–6
- [119] Daami A, Olivier F, Dupré L, Henry F and Templier F 2018 59–4: Invited Paper: Electro-optical size-dependence investigation in GaN micro-LED devices *SID Symposium Digest of Technical Papers* pp 790–3
- [120] Chang Keyin K C, Hsin-Hua H and Chien-Hsing H 2016 MicroLED with dielectric side mirror (US20160181476A1)
- [121] Bulashevich K A, Konoplev S S and Karpov S Y 2018 Effect of die shape and size on performance of III-nitride micro-LEDs: A modeling study *Photonics* **5** 41
- [122] Xie E *et al* 2017 Design, fabrication, and application of GaN-based micro-LED arrays with individual addressing by N-electrodes *IEEE Photonics J.* **9** 7907811
- [123] Virey E H and Baron N 2018 45-1: Status and Prospects of microLED Displays *SID Symposium Digest of Technical Papers* pp 593–6
- [124] Wu T, Sher C W, Lin Y, Lee C F, Liang S, Lu Y, Chen S W H, Guo W, Kuo H C and Chen Z 2018 Mini-LED and micro-LED: promising candidates for the next generation display technology *Appl. Sci.* **8** 1557
- [125] Bower C A *et al* 2017 Emissive displays with transfer-printed assemblies of  $8 \mu\text{m} \times 15 \mu\text{m}$  inorganic light-emitting diodes *Photonics Res.* **5** A23
- [126] Bibl A, Higginson J A, Law H-F S and Hu H-H 2012 Micro device transfer head heater assembly and method of transferring a micro device (US8349116B1)
- [127] Andreas B, Higginson J A, Law H-F S and Hu H-H 2013 Micro device array for transfer to a receiving substrate (US8558243B2)
- [128] Cok R S *et al* 2017 Inorganic light-emitting diode displays using micro-transfer printing *J. Soc. Inf. Disp.* **25** 589–609
- [129] Meitl M A, Zhu Z-T, Kumar V, Lee K J, Feng X, Huang Y Y, Adesida I, Nuzzo R G and Rogers J A 2006 Transfer printing by kinetic control of adhesion to an elastomeric stamp *Nat. Mater.* **5** 33–38
- [130] Sheng X *et al* 2014 Printing-based assembly of quadruple-junction four-terminal microscale solar cells and their use in high-efficiency modules *Nat. Mater.* **13** 593–8
- [131] Meitl M *et al* 2016 55-1: invited paper : passive matrix displays with transfer-printed microscale inorganic LEDs *SID Symposium Digest of Technical Papers* pp 743–6
- [132] Marinov V R 2018 52-4: Laser-Enabled Extremely-High Rate Technology for μLED Assembly *SID Symposium Digest of Technical Papers* pp 692–5
- [133] Lee D, Cherekdjian S, Kang S, Mishra K, Ong P and Xu X 2019 18-2: Ultra-Fine High Efficiency MicroLEDs with Testability and Transferability Using Layer-Transfer Technology *SID Symposium Digest of Technical Papers* pp 236–9
- [134] Henley F J 2019 18-1: Invited Paper: Evaluating In-Process Test Compatibility of Proposed Mass-Transfer Technologies to Achieve Efficient, High-Yield MicroLED Mass-Production *SID Symposium Digest of Technical Papers* pp 232–5
- [135] Henley F J 2018 52-3: Invited Paper: Combining Engineered EPI Growth Substrate Materials with Novel Test and Mass-Transfer Equipment to Enable MicroLED Mass-Production *SID Symposium Digest of Technical Papers* pp 688–91
- [136] Corbett B, Loi R, Zhou W, Liu D and Ma Z 2017 Transfer print techniques for heterogeneous integration of photonic components *Prog. Quantum Electron.* **52** 1–17
- [137] Sasaki K, Schuele P J, Ulmer K and Lee J-J 2017 System and method for the fluidic assembly of emissive displays (US20170133558A1)
- [138] Saeedi E, Kim S S and Parviz B A 2007 Self-assembled inorganic micro-display on plastic 2007 IEEE 20th Int. Conf. on Micro Electro Mechanical Systems (MEMS) pp 755–8
- [139] Bernard J, Haas H, Caplet S, Bedoin A, Tournaire M and Peray P 2019 18-4: microLED displays based on transfer with microtubes interconnections *SID Symposium Digest of Technical Papers* pp 244–7
- [140] Templier F and Bernard J 2019 18-3: A New Approach for Fabricating High-Performance MicroLED Displays *SID Symposium Digest of Technical Papers* pp 240–3
- [141] Peng D, Zhang K, Chao V S D, Mo W, Lau K M and Liu Z 2016 Full-color pixelated-addressable light emitting diode on transparent substrate (LEDoTS) micro-displays by CoB *J. Disp. Technol.* **12** 742–6
- [142] Yeh P 2009 Optics of Liquid Crystal Displays 2nd edn (New York: John Wiley and Sons) pp 792
- [143] Shin W-S, Ahn H-A, Na J-S, Hong S-K, Kwon O-K, Lee J-H, Um J-G, Jang J, Kim S-H and Lee J-S 2017 A driving method of pixel circuit using a-IGZO TFT for suppression of threshold voltage shift in AMLED displays *IEEE Electron Device Lett.* **38** 760–2
- [144] Liou J C and Yang C F 2018 Design and fabrication of micro-LED array with application-specific integrated circuits (ASICs) light emitting display *Microsyst. Technol.* **24** 4089–99
- [145] Yeo K S, Ng W X, Soh M Y and Teo T H 2017 Micro-LED arrays for display and communication: device structure and driver architecture 2017 IEEE 12th Int. Conf. on ASIC (ASICON) pp 993–6
- [146] Sze S M and Ng K K 2006 *Physics of Semiconductor Devices* (New York: John Wiley and Sons) 3rd edn (<https://doi.org/10.1007/b117561>)
- [147] Herrnsdorf J *et al* 2015 Active-matrix GaN micro light-emitting diode display with unprecedented brightness *IEEE Trans. Electron Devices* **62** 1918–25
- [148] Peng D, Zhang K and Liu Z 2017 Design and fabrication of fine-pitch pixelated-addressed micro-LED arrays on printed circuit board for display and communication applications *IEEE J. Electron Devices Soc.* **5** 90–94
- [149] Ahn H A, Hong S K and Kwon O K 2018 An active matrix micro-pixelated LED display driver for high luminance uniformity using resistance mismatch compensation method *IEEE Trans. Circuits Syst. II* **65** 724–8

- [150] Hekmatshoar B, Kattamis A Z, Cherenack K H, Long K, Chen J-Z, Wagner S, Sturm J C, Rajan K and Hack M 2008 Reliability of active-matrix organic light-emitting-diode arrays with amorphous silicon thin-film transistor backplanes on clear plastic *IEEE Electron Device Lett.* **29** 63–66
- [151] Zhang K, Peng D, Chong W C, Lau K M and Liu Z 2016 Investigation of photon-generated leakage current for high-performance active matrix micro-LED displays *IEEE Trans. Electron Devices* **63** 4832–8
- [152] Chong W C, Cho W K, Liu Z J, Wang C H and Lau K M 2014 1700 pixels per inch (PPI) passive-matrix micro-LED display powered by ASIC *Technical Digest—IEEE Compound Semiconductor Integrated Circuit Symp., CSIC* (Institute of Electrical and Electronics Engineers Inc.) (<https://doi.org/10.1109/csics.2014.6978524>)
- [153] Jin S, Choe Y, Lee S, Kim T-W, Mativenga M and Jang J 2016 Lateral grain growth of amorphous silicon films with wide thickness range by blue laser annealing and application to high performance poly-Si TFTs *IEEE Electron Device Lett.* **37** 291–4
- [154] Kim H-M *et al* 2018 66-4: high brightness active matrix micro-LEDs with LTPS TFT backplane *SID Symposium Digest of Technical Papers* pp 880–3
- [155] Liou J C 2018 Circuitry of multiplexer-on-chip system within the micro-LED array manufacturing CMOS substrate *Opt. Quantum Electron.* **50** 400
- [156] Huang Y, Zhang Y, Yin Z, Cui G, Liu H C, Bian L, Yang H and Zhang Y 2011 Indium bump array fabrication on small CMOS circuit for flip-chip bonding *J. Semicond.* **32** 115014
- [157] Li X, Wu L, Liu Z, Hussain B, Chong W C, Lau K M and Yue C P 2016 Design and characterization of active matrix LED microdisplays with embedded visible light communication transmitter *J. Lightwave Technol.* **34** 3449–57
- [158] Choi C, Colón-Berrios A R, Hamachi L S, Owen J S, Schwartz T H, Ma H and Kymmissis I 2018 Localizing seizure activity in the brain using implantable micro-LEDs with quantum dot downconversion *Adv. Mater. Technol.* **3** 1700366
- [159] Zhang X, Li P, Zou X, Jiang J, Yuen S H, Tang C W and Lau K M 2019 Active matrix monolithic LED micro-display using GaN-on-Si epilayers *IEEE Photonics Technol. Lett.* **31** 865–8
- [160] Choi H W, Liu C, Gu E, McConnell G, Girkin J M, Watson I M and Dawson M D 2004 GaN micro-light-emitting diode arrays with monolithically integrated sapphire microlenses *Appl. Phys. Lett.* **84** 2253–5
- [161] Demory B, Chung K, Katcher A, Sui J, Deng H and Ku P-C 2018 Integrated parabolic nanolenses on MicroLED color pixels *Nanotechnology* **29** 165201
- [162] Gong Z *et al* 2012 Electrical, spectral and optical performance of yellow-green and amber micro-pixelated InGaN light-emitting diodes *Semicond. Sci. Technol.* **27** 015003
- [163] Lam H-M, Wang Y, Zhang M, Jiao H and Zhang S 2018 A compact pixel circuit for externally compensated AMOLED displays *IEEE J. Electron Devices Soc.* **6** 936–41
- [164] Yao R-H, Zhang L-R, Zhou L and Wu W-J 2013 A new compensation pixel circuit with all-p-type TFTs for AMOLED displays *Displays* **34** 187–91
- [165] Qiu H, Lu W, Zhang S and Jiao H 2018 P-54: A Low-Power Time-Interleaving Analog Adder for Externally Compensated AMOLED/Micro-LED Displays *SID Symposium Digest of Technical Papers* pp 1399–402
- [166] Ahn H-A, Hong S-K and Kwon O-K 2016 A fast switching current regulator using slewing time reduction method for high dimming ratio of LED backlight drivers *IEEE Trans. Circuits Syst. II* **63** 1014–8